Structural and Functional Implications of Metal Ion Selection in Aminopeptidase P, a Metalloprotease with a Dinuclear Metal Center†

Stephen C. Graham, Charles S. Bond,‡ Hans C. Freeman,* and J. Mitchell Guss*

School of Molecular and Microbial Biosciences, University of Sydney, NSW 2006, Australia

Received July 5, 2005; Revised Manuscript Received August 18, 2005

ABSTRACT: The effect of metal substitution on the activity and structure of the aminopeptidase P (APPro) from *Escherichia coli* has been investigated. Measurements of activity in the presence of Mn^{2+}, Mg^{2+}, Zn^{2+}, Na^{+}, and Ca^{2+} show that significant activity is seen only in the Mn-bound form of the enzyme. The addition of Zn^{2+} to [MnMn(APPro)] is strongly inhibitory. Crystal structures of [MnMn(APPro)], [MgMg-(APPro)], [ZnZn(APPro)], [ZnMg(APPro)], [Ca__(APPro)], [Na__(APPro)], and [*apo*(APPro)] were determined. The structures of [Ca__(APPro)] and [Na__(APPro)] have a single metal atom at their active site. Surprisingly, when a tripeptide substrate (ValProLeu) was soaked into [Na__(APPro)] crystals in the presence of 200 mM Mg^{2+}, the structure had substrate, but no metal, bound at the active site. The structure of *apo* APPro complexed with ValProLeu shows that the N-terminal amino group of a substrate can be bound at the active site by carboxylate side chains that normally bind the second metal atom, providing a model for substrate binding in a single-metal active enzyme. Structures of [MnMn(APPro)] and [ZnZn-(APPro)] complexes of ProLeu, a product inhibitor, in the presence of excess Zn reveal a third metal-binding site, formed by two conserved His residues and the dipeptide inhibitor. A Zn atom bound at such a site would stabilize product binding and enhance inhibition.

Aminopeptidase P (APPro)[1] is a metalloprotease that cleaves the N-terminal amino acid residue from a polypeptide, provided that the second residue is proline. This substrate preference is important, because many biologically active peptides have Xaa-Pro at the N-terminus. For example, APPro plays a direct role in the regulation of the potent vasodilatory mammalian peptide hormone bradykinin (*1*). The presence of APPro in the minimal genomes of *Haemophilus influenzae* and *Mycoplasma genitalium* highlights its importance as an essential enzyme for the recycling of cellular peptides (*2*, *3*).

The molecular structure of APPro is known from high-resolution crystal structure analyses of the native *Escherichia coli* enzyme in three crystal forms (*4*, *5*). The molecule is a tetramer, in which each of the four subunits has a catalytic site centered on a dinuclear Mn(II) cluster. The metal atoms of the cluster are not structurally equivalent: one (Mn_A) is five-coordinate with a distorted square pyramidal geometry, and the other (Mn_B) is six-coordinate with a distorted octahedral geometry. A bridging solvent atom, assumed to be a hydroxide ion at the optimal pH for the enzyme reaction (pH 8), is likely to be the nucleophile that attacks the substrate at the C(peptide) atom of the scissile bond (*4*). The structure of APPro has been solved previously in complex with the product dipeptide ProLeu and the substrate-like inhibitor apstatin (*4*, *6*). These studies identified the substrate binding pocket of APPro: the S_1 site (Tyr229, His243, Asp260, Asp271, His354, Val360, and His361); the S_1' site (Leu242, His243, Asp260, His350, Glu383, and Arg404); and the S_2' site (Arg153, Arg370, Tyr366, Gly351, and His354). The sites are defined according to the nomenclature of Schechter and Berger (*7*). S_1' is the site occupied by the Pro residue of the substrate.

In the present work, we address two important outstanding questions: why is the catalytic activity of APPro promoted better by active site Mn(II) than by other metal atoms? and are both of the metal atoms at the active site cluster equally important for catalytic activity? Previous answers to these questions have been equivocal. Early studies on naturally abundant APPro purified from *E. coli* showed that the enzyme is activated optimally by Mn(II), and weakly by Co-(II), Ni(II), and Cd(II) (*8*). Recombinant *E. coli* APPro has been reported to be fully activated by Mn(II) and weakly by trace amounts of Zn(II) (*9*). Human cytosolic APPro and membrane-bound rat lung APPro are also activated strongly by Mn(II), less so by Co(II), and not at all by Ca(II), Mg-

† This work was supported by the Australian Research Council (DP0208320, J.M.G. and H.C.F.). S.C.G. is the recipient of an Australian Postgraduate Award. Access to the Stanford Synchrotron Radiation Laboratory was supported by a travel grant from the Access to Major Research Facilities Program administered by the Australian Nuclear Science & Technology Organisation. Amino acid analysis was facilitated by access to the Australian Proteome Analysis Facility established under the Australian Government's Major National Research Facilities program.

* To whom correspondence should be addressed. H.C.F.: e-mail, freemanh@chem.usyd.edu.au; tel, +61 2 9351 6028. J.M.G.: e-mail, m.guss@mmb.usyd.edu.au; tel, +61 2 9351 4302; fax, +61 2 9351 4726.

‡ Present address: Division of Biological Chemistry and Molecular Microbiology, School of Life Sciences, Wellcome Trust Biocentre, University of Dundee, Dundee DD1 5EH, U.K.

[1] Abbreviations: APPro, aminopeptidase P; CBVS, calcium bond valence sum; EDTA, ethylenediaminetetraacetic acid; EGTA, ethylene glycol-bis(2-aminoethyl ether)-*N*,*N*,*N*′,*N*′-tetraacetic acid; ICP-MS, inductively coupled plasma mass spectrometry; MetAP, methionine aminopeptidase; MPD, 2-methyl-2,4-pentanediol; PEG, poly(ethylene glycol).

10.1021/bi0512849 CCC: $30.25
Published on Web 09/28/2005

(II), and Zn(II) (*10*−*12*). Spectroscopic measurements on *E. coli* APPro are consistent with a substantial difference between the affinities of the enzyme for the first and second Mn(II) atoms of the dinuclear cluster (*13*), and human cytosolic APPro recombinantly expressed in *E. coli* is active when it contains only one molar equivalent of Mn(II) (*11*). The situation is complicated further by an observation that porcine membrane-bound APPro is activated by one molar equivalent of Zn(II) (*14*). It is unlikely that the reported differences among the cited APPros arise from different active site clusters, since an alignment of APPro sequences shows that the metal-binding residues are strictly conserved (*6*).

Similar questions concerning the essential features of a dinuclear metal site arise in the case of two related enzymes. APPro belongs to a small family of 'pita-bread' metalloaminopeptidases, named for the conserved polypeptide fold of the catalytic domain. The other known members of the family are prolidase, which is specific for Xaa-Pro dipeptide substrates, and methionine aminopeptidase (MetAP), which cleaves oligopeptides with a Met-Xaa N-terminus. The structures of prolidase and MetAP have been determined. Both enzymes have an active site centered on a dinuclear metal cluster with the same metal-binding residues as in APPro. Prolidase has been identified as Co(II)-dependent (*15*). The Zn(II)-enzyme is inactive (*16*). In the case of MetAP, the metal required to potentiate the enzyme was originally also identified as Co(II) (*17*), but later experimental evidence has favored Zn(II) for type-I yeast MetAP (*18*), Fe(II) for *E. coli* MetAP (*19*), and Mn(II) for human type-II MetAP (*20*). For both prolidase and MetAP, there is strong evidence that the two metal atoms in the dinuclear cluster have different effects on the catalytic reaction. Prolidase is inactive with one Co(II) atom and requires a second Co(II) atom for activity (*15*). For *E. coli* MetAP, spectroscopic and kinetics data show that one of the metal sites is 'tight', and the other 'loose' (*21*). Under anaerobic conditions, catalysis occurs when only the 'tight' metal-binding site is occupied by Co(II) or Fe(II) (*21*, *22*). Occupancy of the 'loose' metal-binding site by Co(II) or Fe(II) affects the kinetic activity negatively (see ref *23* for a review).

To explore these two key questions further in relation to APPro, we have solved and refined the crystal structures of [MgMg(APPro)], [ZnZn(APPro)], [ZnMg(APPro)], [Ca_(APPro)], [Na_(APPro)], and [*apo*(APPro)]. To provide a baseline for structural comparisons, the original [MnMn(APPro)] structure has been re-refined with improved protocols. The activity of *E. coli* APPro has been measured after incubating the *apo*-enzyme with Mn^{2+}, Mg^{2+}, Zn^{2+}, and Ca^{2+}. The structures of complexes prepared by exposing crystals of APPro to a tripeptide substrate, ValProLeu, or a dipeptide hydrolysis product, ProLeu, have also been determined. On the basis of these experiments, we are able to suggest reasons why the Mg(II)-, Ca(II)-, and Na(I)-loaded forms of the enzyme are inactive and why the active Mn(II) enzyme is inhibited by Zn^{2+}.

MATERIALS AND METHODS

Protein Expression and Purification. Several different samples of *E. coli* APPro were prepared during the course of the experiments described in this work. The protein was overexpressed in *E. coli* AN1459/pPL670 as previously reported (*13*). The protein was purified either by the previously reported method (sample 1) (*4*, *13*) or by small modifications thereof. Sample 1: lysed cells were subject to $(NH_4)_2SO_4$ precipitation at 4 °C followed by centrifugation. The pellet was resuspended and applied to a DEAE−Fractogel column (Merck). The APPro-containing fraction was then passed over a ceramic hydroxyapatite column (Bio-Rad). The sample was then dialyzed twice against 1 L of 20 mM Tris (pH 7.6) and 1.5% (w/v) DTT. The protein was concentrated to 5.7 mg mL^{-1} as determined by amino acid analysis. Sample 2: additional steps were taken to remove any bound metal ions. After hydroxyapatite chromatography, the protein was dialyzed twice against 2 L of 20 mM Tris (pH 8.5), 1.5% (w/v) DTT, and 1 mM EDTA and then against 2 × 2 L of 20 mM Tris (pH 8.5) and 1.5% (w/v) DTT. Protein was concentrated to 10 mg mL^{-1} as determined by a Coomassie dye-binding assay (Bio-Rad). Sample 3: a modified protocol, which avoided overnight dialysis, speeded up the purification. After resuspension in 30 mL of 50 mM Tris (pH 8.0) and 0.1 mM EDTA at 4 °C, cells were lysed by incubation with lysozyme at 4 °C for 30 min followed by sonication. The lysate was cleared by ultracentrifugation (100 000*g*, 30 min, 4 °C). Cleared cell lysate was diluted to 100 mL in 20 mM Tris (pH 7.6), applied to an anion exchange column (Toyoperl DEAE-650M, Tosoh, Japan), and eluted against a gradient of 20 mM Tris (pH 7.6) and 1 M NaCl. Pooled eluate was combined with an equal volume (30 mL) of 20 mM Tris (pH 7.6) and 3 M $(NH_4)_2SO_4$ and centrifuged (27 000*g*, 10 min) before being applied to an EconoPac Methyl-HIC cartridge (Bio-Rad) and eluted against a gradient of 20 mM Tris (pH 7.6). Pooled HIC eluate was concentrated (30 kDa MWCO, Millipore) and then dialyzed (Slide-A-Lyzer 10 kDa MWCO, Pierce) against 3 × 1 L of 20 mM Tris (pH 7.6) and 1 mM EGTA at 4 °C. The final APPro concentration was 7.7 mg mL^{-1} as determined by a Coomassie dye-binding assay (Bio-Rad).

Peptide Synthesis. ValProLeu was manually synthesized by solid-phase methods using Fmoc chemistry. Starting materials and reagents were purchased from Auspep (Australia). Following cleavage from the resin with trifluoroacetic acid, the peptide was purified by HPLC using a C_{18} column (Varian). The identity of the purified peptide was verified by electrospray mass spectrometry (Finnigan LCQ).

Protein Crystallization. Crystals were grown at 4 °C by vapor diffusion in hanging drops containing 3 μL of precipitant solution and 3 μL of 10 mg mL^{-1} APPro unless stated otherwise. Crystals generally grew in 1 or 2 weeks.

Hexagonal crystals of [*apo*(APPro)] were grown using sample 2 of APPro under conditions similar to those reported previously (0.1 M Tris (pH 8.1) and 30% (w/v) PEG 4K (*4*)). Crystals of [MgMg(APPro)] were prepared from [*apo*(APPro)] crystals by soaking for 1 h in mother liquor supplemented with 100 mM $MgCl_2$. Orthorhombic crystals of [Ca_(APPro)] were grown under conditions similar to those reported previously (25% (w/v) PEG 4K, 0.2 M Na acetate, 0.1 M Tris (pH 8.5), and 0.1 mM EDTA (*5*)) using sample 2 of APPro. The Ca^{2+} was introduced in the buffer used for cryoprotection (see below). Tetragonal crystals of [Na_(APPro)] were grown at 4 °C in sitting drops containing 2 μL of reservoir solution (26% (v/v) MPD, 0.1 M Na citrate (pH 7.0−7.5), and 0.2 M Mg acetate) and 2 μL of APPro (sample 3). Crystal samples of [*apo*(APPro) + ValProLeu]

and [MgMg(APPro) + ProLeu] were prepared by soaking [Na_(APPro)] crystals in fresh drops of mother liquor with added 10 mM ValProLeu for 1 and 20 h, respectively. Crystals of [ZnZn(APPro)] and [ZnZn(APPro) + ProLeu] were prepared by soaking [Na_(APPro)] crystals for 2 h in mother liquor with added 1 mM $ZnCl_2$ with and without 10 mM ProLeu dipeptide (Sigma). Crystals of [MnMn(APPro) + Zn, ProLeu] were prepared from [Na_(APPro)] crystals by soaking for 1 h in mother liquor with added 1 mM $MnCl_2$, 1 mM $ZnCl_2$, and 10 mM ProLeu (Sigma).

Monoclinic crystals of [ZnMg(APPro)] were grown at 20 °C in hanging drops containing 3 μL of reservoir solution (16% (w/v) PEG4K, 0.1 M Tris (pH 8.3), and 0.2 M $MgCl_2$), 2 μL of APPro (sample 1), and 0.55 μL of 0.2 M $MgCl_2$. Peptide complexes of [ZnMg(APPro)] were prepared by soaking crystals overnight in fresh drops containing mother liquor supplemented with 15% (v/v) MPD and 10 mM ValProLeu. No Zn was added to any of the buffers used for crystallization or for cryoprotection of the monoclinic crystals.

X-ray Diffraction Data. Crystals that had been grown in a solution containing MPD or had been transferred to a solution of peptide with added MPD required no further cryoprotection prior to flash cryo-cooling. Crystals of [*apo*(APPro)] and [MgMg(APPro)] were cryoprotected by brief washing in mother liquor containing 20% (v/v) 2-propanol or 20% (v/v) 2-propanol with added $MgCl_2$, respectively. Similarly, crystals of [ZnMg(APPro)] were cryoprotected by a brief wash with 20% (v/v) MPD in the mother liquor. Crystals of [Ca_(APPro)] were transferred to fresh mother liquor supplemented with 5 mM $CaCl_2$ for 10 min and then cryoprotected by brief washing in successive solutions containing $CaCl_2$-supplemented mother liquor and concentrations of 2-propanol increasing from 10% to 30% (v/v).

All crystals were flash cryo-cooled in a stream of N_2 gas prior to data collection. Diffraction data were recorded at 100 K. Laboratory data were recorded with X-rays produced by a Rigaku RU200H rotating anode generator (Cu Kα, 1.5418 Å). Diffraction data for [*apo*(APPro)], [MgMg(APPro)], and [Ca_(APPro)] crystals were recorded on a Rigaku R-axis IIC imaging plate system with Yale mirror optics. Diffraction data for all other crystals other than [ZnMg(APPro) + ProLeu] were recorded on a Mar345 imaging plate with Osmic optics. Diffraction data for [ZnMg(APPro) + ProLeu] were recorded at the Stanford Synchrotron Radiation Laboratory beamline 9-2 on an ADSC Quantum-315 CCD detector. Data were recorded from a single crystal using X-rays at two wavelengths above and below the Zn Kα absorption edge: 1.2817 Å (9673 eV) and 1.2861 Å (9640 eV), respectively. All diffraction images were indexed and integrated using DENZO, and the data were scaled using SCALEPACK (*24*).

Structure Solution and Refinement. The 12 structures in this paper were refined by slight variations of the same protocol. The starting models were stripped of metal atoms, solvent atoms, hetero compounds, and residues with multiple conformations. The models were originally treated as single rigid bodies and refined with REFMAC5 to 3 Å resolution. Further rounds of refinement involved manual model building with O (*25*) or COOT (*26*), using sigma-A weighted electron-density maps (*27*), followed by TLS (*28*) and restrained refinement with REFMAC5 using all data (*29*). The structure of native APPro ([MnMn(APPro)]) was re-refined using the published structure (PDB ID 1AZ9 (*4*)) as the starting model. The structures of [*apo*(APPro)] and [MgMg(APPro)] were refined using the re-refined [MnMn(APPro)] structure (PDB ID 1WL9) as the starting model. The structure of [Ca_(APPro)] was refined using the isomorphous structure of native APPro refined in the orthorhombic space group $C222_1$ (PDB ID 1M35 (*5*)) as the starting model. Initial rigid-body refinement treated each of the six monomers in the asymmetric unit as a separate rigid body. Initially, NCS restraints were applied to all residues in the six independent chains. In the final rounds of refinement, these restraints were removed in those parts of the polypeptide chains affected by crystal packing. All structures of APPro crystallized in the tetragonal space group $I4_122$ were refined using the isomorphous structure of native APPro in complex with apstatin (PDB ID 1N51 (*6*)) as the starting model.

The structure of [ZnMg(APPro)] was solved by molecular replacement using the program AMORE (*30*). The search model was a tetramer of the re-refined [MnMn(APPro)] structure generated from a monomer by crystal symmetry, stripped of all metal atoms, solvent atoms, residue modifications, and multiple conformers. Two solutions were clearly distinguished by lower *R*-values and higher figures of merit. Inspection of unit cell packing showed that each tetramer lay on a crystallographic two-fold axis. It was therefore concluded that the asymmetric unit contained 2 dimers (4 monomers) of APPro. The tetramers are generated by crystallographic two-fold axes. Initial rigid body refinement treated each of the 4 monomers in the asymmetric unit as a separate rigid body. In early rounds of TLS and restrained refinement, NCS restraints between the 4 monomers were applied to all residues. These restraints were removed in the later rounds of refinement for residues involved in crystal-packing contacts.

Analysis and validation of all structures was performed with the aid of PROCHECK (*31*), SFCHECK (*32*), WHATCHECK (*33*), and MOLPROBITY (*34*). The refinement restraints for the modified cysteine residues and other hetero compounds were created with the assistance of the PRODRG (*35*) and HIC-UP (*36*) servers. Superpositions and comparisons of C^{α} positions were performed using LSQMAN (*37*). Peaks in anomalous electron-density difference maps were integrated with MAPMAN (*38*) in $2 \times 2 \times 2$ Å^3 boxes centered on the peak maximum.

Metal Ion and Protein Analyses. ICP-MS analysis was performed on a Hewlett-Packard 4500 Inductively Coupled Plasma Mass Spectrometer. Amino acid analysis was carried out using gas-phase hydrolysis and Waters AccQTag chemistry. Cysteine and tryptophan concentrations, not measurable by this technique, were calculated from known sequence data.

Enzyme Kinetics. Activity of APPro was assayed using a quenched fluorescent substrate Lys(Abz)-Pro-Pro-pNA (Bachem, Switzerland) (*39*). The appearance of fluorescent product ($\lambda_{ex} = 340$ nm, $\lambda_{em} = 430$ nm) was measured on a Wallac Victor^2 1420 fluorescent plate reader (Perkin-Elmer). All assays were performed in black 96-well polypropylene plates (Greiner bio-one, Germany) with a final assay volume of 250 μL. IC_{50} values were estimated by fitting a sigmoidal dose−response curve to the experimental data by nonlinear

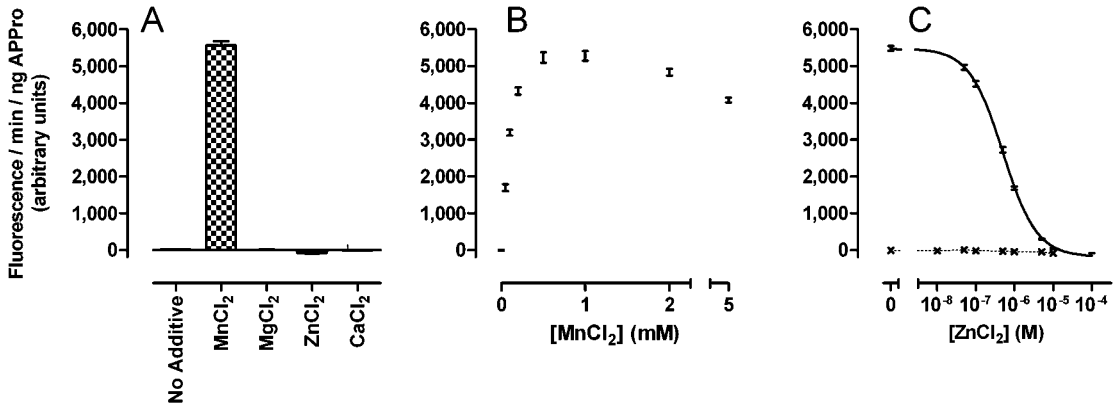

FIGURE 1: Activity of *E. coli* APPro. The activity is shown as arbitrary fluorescence units. All assays were performed at 37 °C for 30 min in the presence of 50 mM Tris (pH 8.1), 100 mM NaCl, 100 μM Lyz(Abz)-Pro-Pro-pNA quenched fluorescent substrate, and 1 μg mL^{-1} APPro that had been dialyzed overnight against EGTA (sample 3). Standard errors are shown ($n = 5$). (A) Activity of APPro in the presence of different metal salts (1 mM); (B) activity of APPro as a function of $MnCl_2$ concentration; and (C) activity of APPro as a function of $ZnCl_2$ concentration. Assays in panel C were performed in the presence of 1 mM $MnCl_2$ (solid line) and in the absence of $MnCl_2$ (dotted line, errors too small to be shown on this scale).

regression using the program PRISM 4 (Graph Pad Software).

RESULTS

The Effect of Metal Ions on the Activity of APPro. As has been observed previously (*40*), *E. coli* APPro that is dialyzed against a buffer containing EGTA (sample 3, $[APPro]_{assay} = 20$ nM) to remove divalent metal ions is not active (Figure 1A). The buffers used in these kinetics assays were analyzed for the presence of Fe^{2+}, Co^{2+}, Mn^{2+}, or Zn^{2+}, which have been reported to activate APPro. All were below detectable levels by ICP-MS. Among the metal ions studied (Ca^{2+}, Mg^{2+}, Mn^{2+}, Na^{+}, and Zn^{2+}), the only significant activity was found in the presence of Mn^{2+} (Figure 1A). Slight inhibition was observed when the concentration of Mn^{2+} exceeded 1 mM (Figure 1B). In the absence of added Mn^{2+}, low levels of APPro activity were observable only when the concentration of enzyme was raised to at least 50 times the level used in the standard assay (deposited as Supporting Information).

Zn^{2+} strongly inhibits fully active Mn-loaded APPro ($IC_{50} = 0.5$ μM, Figure 1C). Zn^{2+} is not able to activate APPro, even at concentrations below those at which it inhibits the Mn-loaded active enzyme (Figure 1C).

Molecular Structure of APPro in the Presence of Different Metals. The structures of APPro with different active site metals ([MnMn(APPro)], [MgMg(APPro)], [ZnMg(APPro)], [ZnZn(APPro)], [Ca__(APPro)], and [Na__(APPro)]), in the absence of metals ([*apo*(APPro)]), in the presence of substrate ([*apo*(APPro) + ValProLeu]), and in the presence of product ([MgMg(APPro) + ProLeu], [ZnMg(APPro) + ProLeu], [ZnZn(APPro) + Zn, ProLeu], and [MgMg(APPro) + Zn, ProLeu]) have been refined (Table 1). All but the two [ZnMg(APPro)] structures crystallized in the hexagonal ($P6_4$22), tetragonal ($I4_1$22), and orthorhombic ($C222_1$) space groups previously observed for APPro (*4*, *5*). [ZnMg(APPro)] and [ZnMg(APPro) + ProLeu] crystallized in the monoclinic space group, $C2$ (Table 1). No significant differences in tertiary or quaternary structure of APPro are observed in comparisons between any of these structures. Excluding the two C-terminal residues Lys439 and Gln440, which do not adopt a single conformation, the rms differences between the positions of 438 corresponding C^{α} atoms in the native [MnMn(APPro)] and derivative APPro structures range from 0.10 to 0.34 Å.

Very few residues in the substrate-binding cleft of APPro adopt different conformations despite differences between the contents of the active sites. Metal−ligand residues undergo only minor shifts in response to the presence of different metal atoms at the active site (see below). Among the residues in the substrate-binding pocket, only His243 responds to changes at the active site (see Discussion).

In several of the structures presented, there is evidence for oxidation of the sulfhydryl group of Cys249 (Figure 2). In [MnMn(APPro)] and [Ca__(APPro)], Cys249 is oxidized to a sulfenic acid (Cys-SOH). In [ZnMg(APPro)] and [ZnMg(APPro) + ProLeu], Cys249 is fully oxidized to a sulfonic acid (Cys-SO_3). Oxidation of cysteine sulfhydryl groups has been observed previously in protein crystal structures (*41*).

Several features appear consistently in all the structures which crystallize in a given space group. For example, in the hexagonal, orthorhombic, and monoclinic crystals but not in the tetragonal crystals, a chloride ion is present between the N(peptide) atoms of residues 111 and 80. This ion has been identified positively by the presence of significant anomalous difference electron density and by the height of positive difference electron density. When a water molecule is modeled at this position, its temperature factor refines to the minimum limit and significant positive difference electron density remains.

In tetragonal crystals of APPro, an Mg(II) atom is located at one of the crystal contacts between adjacent APPro molecules. The atom has been identified as Mg(II) in these structures by the height of the peak in difference density and by the lack of anomalous difference density. This site was modeled as an Mn(II) atom with 0.5 occupancy in [MnMn(APPro) + apstatin] (*6*). The Mg(II) atom is coordinated by six solvent atoms in an octahedral geometry, which in turn form hydrogen bonds with an O(carboxylate) atom of Glu396, the O(peptide) atoms of Glu396, Gln397, and Arg399, the O(peptide) atom of Asp253 in a subunit of an adjacent tetramer (generated by the symmetry operation [x, 1/2 − y, 1/4 − z]), and several solvent molecules. The

Table 1: Data Collection and Refinement Statistics

crystal	[MnMn(APPro)] (native)	*apo* APPro	[MgMg(APPro)]	[Ca_(APPro)]	[Na_(APPro)]	*apo* APPro + ValProLeu	[MgMg(APPro) + ProLeu[a]]	[ZnZn(APPro)]	[ZnZn(APPro) + Zn, ProLeu[a]]	[ZnZn(APPro) + Zn, ProLeu]	[MnMn(APPro) + Zn, ProLeu]	[ZnMg(APPro)]	[ZnMg(APPro) + ProLeu[a]]
Crystal and Diffraction Data													
pH	8.3	8.1	8.1	8.5	7.5	7.5	7.5	7.0	7.5	7.0	7.5	8.3	8.3
space group	$P6_422$	$P6_422$	$P6_422$	$C222_1$	$I4_122$	$I4_122$	$I4_122$	$I4_122$	I_122	$I4_122$	$I4_122$	C2	C2
unit cell dimensions													
a (Å)	177.42	177.32	177.73	208.36	138.78	138.22	138.57	138.81	138.99	138.01	139.69	111.97	111.73
b (Å)	–	–	–	312.69	–	–	–	–	–	–	–	236.70	236.53
c (Å)	96.42	96.31	96.48	160.20	231.01	230.84	230.96	230.91	230.74	230.73	230.67	137.64	138.00
β (deg)	–	–	–	–	–	–	–	–	–	–	–	106.14	106.34
X-ray source	rotating anode	rotating anode	rotating anode	rotating anode	rotating anode	rotating anode	rotating anode	rotating anode	rotating anode	rotating anode	rotating anode	rotating anode	SSRL 9-2
λ (Å)	1.5418	1.5418	1.5418	1.5418	1.5418	1.5418	1.5418	1.5418	1.5418	1.5418	1.5418	1.5418	1.2817
detector	Raxis IIc	Raxis IIc	Raxis IIc	Raxis IIc	Mar345	Mar345	Mar345	Mar345	Mar345	Mar345	Mar345	Mar345	Quantum-315
resolution range (Å)	38.9−1.9 (1.97−1.90)[b]	50.0−2.1 (2.18−2.10)	42.0−2.0 (2.05−2.00)	30.0−2.4 (2.48−2.40)	60.0−2.4 (2.49−2.40)	60.0−2.4 (2.49−2.40)	60.0−2.5 (2.59−2.50)	60.0−2.4 (2.49−2.40)	60.0−2.8 (2.90−2.80)	60.0−2.4 (2.49−2.40)	60.0−2.4 (2.49−2.40)	40.0−2.3 (2.38−2.30)	40.0−2.0 (2.07−2.00)
observed reflections	238 899	175 115	183 255	424 315	237 304	221 444	302 908	273 016	269 380	269 380	392 368	419 909	641 136
unique reflections	65 397	47 238	56 227	192 310	43 830	43 763	38 892	43 879	28 154	43 466	44 853	150 182	225 729
completeness (%)	93.0 (63.4)	90.2 (59.4)	92.4 (64.2)	94.5 (86.0)	98.8 (100.0)	99.5 (99.9)	99.2 (100.0)	98.9 (91.0)	99.8 (98.5)	99.2 (98.5)	100.0 (99.7)	98.9 (97.6)	97.9 (96.2)
multiplicity	3.7 (1.5)	3.7 (2.3)	3.3 (1.9)	2.2 (1.9)	5.5 (4.6)	5.1 (4.4)	7.8 (7.0)	6.2 (4.7)	7.4 (6.9)	6.1 (5.0)	8.7 (7.0)	2.8 (2.7)	2.9 (2.7)
$\langle I/\sigma(I)\rangle$	24.4 (5.7)	32.9 (7.2)	26.5 (5.4)	19.6 (4.5)	20.8 (2.6)	20.2 (2.4)	22.7 (3.4)	22.2 (3.4)	16.3 (2.7)	25.2 (3.2)	25.4 (3.2)	17.6 (3.4)	13.9 (6.0)
R_{merge}[c]	0.052 (0.261)	0.059 (0.239)	0.072 (0.333)	0.040 (0.181)	0.074 (0.594)	0.077 (0.626)	0.086 (0.578)	0.066 (0.486)	0.128 (0.671)	0.051 (0.520)	0.067 (0.536)	0.060 (0.324)	0.074 (0.444)
Refinement Statistics													
reflections in working set	63 537	45 746	54 464	182 590	41 640	41 583	36 971	41 450		41 151	42 558	142 654	214 328
reflections in test set	1991	1475	1708	9688	2132	2130	1888	2126		2099	2184	7512	11 297
protomers per ASU	1	1	1	6	1	1	1	1		1	1	4	4
total atoms (non-H)	4125	3990	4160	22 063	3672	3661	3638	3750		3688	3825	14 814	15 192
protein atoms	3500	3499	3499	20 931	3487	3487	3487	3487		3487	3487	13 960	13 964
metal atoms	2	0	2	6	2	1	3	5		5	4	10	10
water atoms	605	456	599	1072	149	109	98	216		146	286	832	1093
atoms in alternate conformers	17	13	19	0	21	28	21	21		21	19	8	57
other atoms[d]	1	22	41	54	13	36	29	21		29	29	4	68
R_{cryst}[e]	0.152 (0.235)	0.150 (0.169)	0.148 (0.201)	0.176 (0.218)	0.177 (0.275)	0.178 (0.266)	0.180 (0.320)	0.168 (0.279)		0.175 (0.258)	0.166 (0.284)	0.168 (0.232)	0.157 (0.230)
R_{free}[f]	0.170 (0.267)	0.180 (0.204)	0.173 (0.220)	0.200 (0.265)	0.202 (0.313)	0.204 (0.337)	0.204 (0.329)	0.190 (0.294)		0.201 (0.297)	0.187 (0.330)	0.197 (0.261)	0.180 (0.252)
rmsd bond lengths (Å)	0.011	0.012	0.011	0.013	0.010	0.011	0.010	0.009		0.009	0.008	0.009	0.009
rmsd bond angles (deg)	1.280	1.290	1.296	1.254	1.141	1.172	1.169	1.113		1.117	1.087	1.070	1.106
$\langle B\rangle$ (Å^2)	18.0	18.8	17.5	26.1	44.8	47.3	43.2	46.6		47.2	48.0	35.1	36.3
DPI (Å)[g]	0.09	0.12	0.10	0.21	0.16	0.16	0.18	0.15		0.16	0.15	0.17	0.10
PDB ID	1WL9	1WLR	1WL6	1W2M	2BHC	2BHA	2BHD	2BHB		2BH3	2BN7	1WBQ	1W7V

[a] The crystal was soaked with substrate (ValProLeu), but only product (ProLeu) was observed at the active site. [b] The values in parentheses are for the highest resolution shell. [c] $R_{merge} = \sum_h\sum_i|I_{hi} - \langle I_h\rangle|/\sum_h\sum_i\langle I_h\rangle$. [d] Includes atoms of bound substrate, product, PEG, buffer, or anions. [e] $R_{cryst} = \sum_h|F_h(obs) - F_h(calc)|/\sum_h F_h(obs)$. [f] $R_{free} = R_{cryst}$ for approximately 5% of the data selected at random for the native structure not used during refinement. The same reflection set, chosen at random, was used for all structures refined in the same space group. [g] DPI is the diffraction precision indicator defined by Cruickshank (*60*).

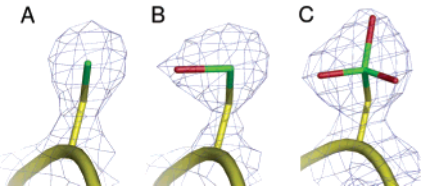

FIGURE 2: Oxidation of Cys249. $2F_O - F_C$ electron density contoured at 1.8σ is shown in blue. (A) [MgMg(APPro)], no oxidation; (B) [MnMn(APPro)], Cys249 is modeled as a sulfenic acid; and (C) [ZnMg(APPro) + ProLeu], Cys249 is modeled as a sulfonic acid. PyMOL was used to prepare molecular images (*61*).

calcium bond valence sum (CBVS) is 4.3 compared with an expected value of 4.2 for Mg^{2+} (cf. Na^+ 1.6, Ca^{2+} 2.0, Mn^{2+} 3.2, and Zn^{2+} 4.1) confirming its identity (*42*). The structures also contain an ordered molecule of citrate, which forms a hydrogen bond with $N^{\delta}1$ (His222) and a salt-bridge with the guanidyl group of Arg186.

Refinement of Native APPro. The structure of native APPro ([MnMn(APPro)]) was refined against the same diffraction data used previously to refine the structure (PDB ID 1AZ9 (*4*)). The resolution of the data was extended from 2.0 to 1.9 Å by including reflections at the corners of the square imaging plate detector, slightly reducing completeness in the outermost shell. The extra data improved the quality of electron-density difference maps. The refinement was further improved by TLS refinement in REFMAC5, which had not been available during the original refinement (*28*). The R and R_{free} values, 0.152 and 0.170, respectively, compare favorably with the previous values, 0.165 and 0.192. The R values are lower despite the presence of fewer solvent molecules in the model (605 versus 742), the use of fixed occupancy (1.0) for solvent atoms, and the inclusion of data to higher resolution. The new refinement has corrected some irregular bond lengths and angles at the active site of the previous model (Figure 3A).

There are a few significant localized differences between the newly refined and previously published structures: the loop between residues 82 and 89, although not well-defined, now forms a short stretch of α-helix. It includes a new hydrogen bond from the O(peptide) atom of Thr84, which previously pointed into the solvent, to the N(peptide) atom of Trp88. The orientations of several side chains far from the active site have been changed to provide a better fit to the electron density, more plausible hydrogen bonding, or better stereochemistry.

The Structure of Apo APPro. Although there are no metal atoms at the active site of [*apo*(APPro)], there are very few significant structural differences from the native structure (Figure 3B). A water molecule (W_A) occupies the M_A site. W_A is surrounded by five potential hydrogen-bond donors and acceptors: $O^{\delta 2}$(Asp271), $O^{\epsilon 2}$(Glu406), $O^{\epsilon 1}$(Glu383), $O^{\epsilon 2}$-(Glu383), and $N^{\epsilon 2}$(His354). Assuming that the interaction between W_A and the side-chain carboxylate group of Glu383 is a three-centered hydrogen bond, a minimum of four protons are required for the observed interactions with Asp271, Glu406, Glu383, and His354. W_A does not have sufficient protons for four hydrogen bonds. Thus, it is likely that one of the neighboring carboxylate side chains is protonated and that W_A is a proton acceptor in the hydrogen bond with $N^{\epsilon 2}$(His354). Since $N^{\delta 1}$(His354) is hydrogen-bonded to the O(peptide) atom of Trp355, it follows that the imidazole group of His354 is doubly protonated. A second water molecule (W_B) at the active site lies between the positions of Mn_B and the bridging hydroxide ion in [MnMn(APPro)]. The electron density for W_B is weak, indicating that it is disordered, and the hydrogen bonds formed by W_B cannot be assigned reliably. The positions of all metal ligand residues are slightly different from those in the [MnMn(APPro)] structure. The main-chain torsion angles, φ and ψ, at Glu270 and Asp271 differ by up to 10°. The position of the side chain of Asp271 differs from its position in [MnMn(APPro)] by nearly 1.0 Å as a result of a 10° rotation around the $C^{\beta}-C^{\gamma}$ bond.

Additional features of [*apo*(APPro)] include an ordered segment of poly(ethylene glycol) (PEG) in the substrate channel, and two molecules of 2-propanol. The PEG segment contains four ethylene glycol repeats of the approximately 90 present in an average PEG 4K molecule. The PEG segment makes hydrophobic contacts with seven residues at the active site including His243 and His361. As a result, His243, which is disordered in [MnMn(APPro)], is well ordered in [*apo*(APPro)]. The two 2-propanol molecules in [*apo*(APPro)] are located far from the active site.

The Structure of MgMg APPro. The active site of [MgMg-(APPro)] is closely similar to that of the native structure. The metal atoms occupy equivalent sites and are bound by the same ligands (Figure 3C). Corresponding metal−ligand bond lengths in the Mg and Mn structures do not differ significantly (Figure 3A,C). However, the metal−water distance M_A−W2 in [MgMg(APPro)], 2.3 Å, is shorter than that in [MnMn(APPro)], 2.8 Å. As a result, Mg_A has a six-coordinate distorted octahedral geometry, instead of the five-coordinate distorted square pyramidal geometry of Mn_A in [MnMn(APPro)]. Mg_B has a six-coordinate distorted octahedral geometry like Mn_B in [MnMn(APPro)], but the bond angles at Mg_B are closer to ideal octahedral geometry. The difference between the metal−water distances Mg_B−W3 and Mn_B−W3, 2.2 and 2.4 Å, is of marginal significance.

Additional features at the active site of [MgMg(APPro)] include an ordered molecule of 2-propanol from the cryo-buffer and an ordered segment of PEG. The hydroxyl group of the 2-propanol makes a hydrogen bond with $N^{\epsilon 2}$(His243), stabilizing the conformation of the imidazole ring. Ten ethylene glycol units from the PEG 4K used in the crystallization buffer form a well-ordered segment at the active site (Figure 4). One end of the PEG segment overlaps with the PEG in [*apo*(APPro)]. The other end of the shorter segment of PEG in [*apo*(APPro)] occupies the position of the 2-propanol in [MgMg(APPro)]. The PEG segment makes hydrogen bonds with the side chain of Arg153 from an adjacent subunit in the tetramer (generated by the symmetry operation [$1 - x$, $1 - y$, z]) and has hydrophobic contacts with the side chains of residues His243, His354, His361, Tyr366, Arg370, and with Trp88 from an adjacent subunit tetramer (generated by the symmetry operation [$1 - y$, $1 - x$, $1^1/_3 - z$]). To accommodate the PEG, the side chain of Arg153 in the neighboring subunit becomes ordered and creates a binding pocket for an additional chloride ion. This chloride ion contacts the N(peptide) atom of His351 as well as the side chains of Arg153 and Arg370.

The Structure of Ca__ APPro. Crystals of [Ca__(APPro)] are isomorphous with the orthorhombic form of the native structure (*5*). There are six molecules in the asymmetric unit,

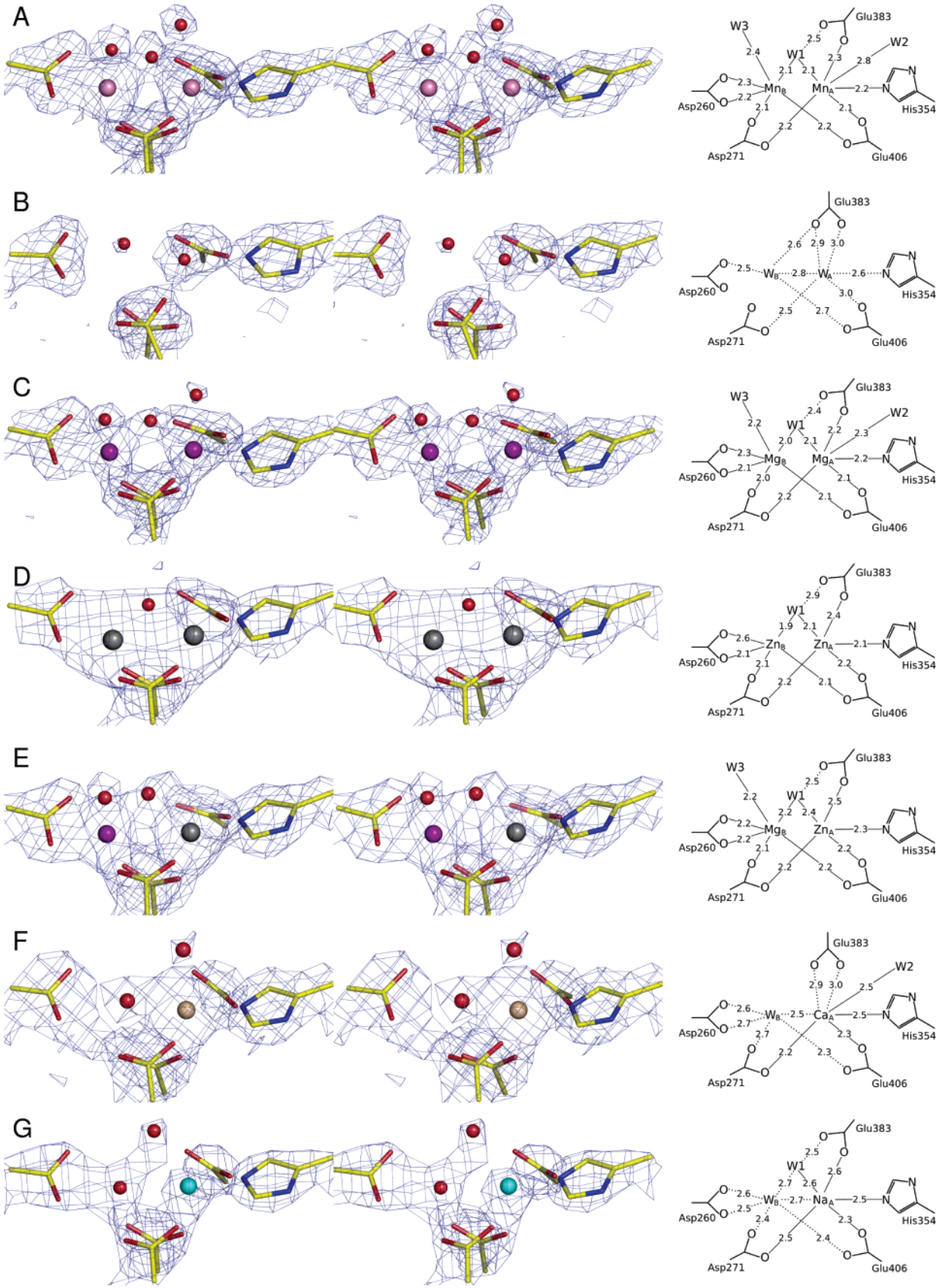

FIGURE 3: Stereoviews showing the active site of *E. coli* APPro in the presence of different metals. $2F_O - F_C$ electron density (2σ for A, C−E, and G; 1.5σ for B and F) is shown in blue. For clarity, only the metal ligand residues are shown. Distances displayed in the right column are in angstroms; average values for the independent copies in the asymmetric unit are shown for E and F. (A) [MnMn(APPro)]; (B) [*apo*(APPro)]; (C) [MgMg(APPro)]; (D) [ZnZn(APPro)]; (E) [ZnMg(APPro)]; (F) [Ca_(APPro)]; and (G) [Na_(APPro)].

designated A−F. One tetramer of APPro is formed by four of the subunits, and the other by the operation of a crystallographic two-fold axis on the remaining two subunits. The C-terminal residues A440, B438−440, C440, and E440

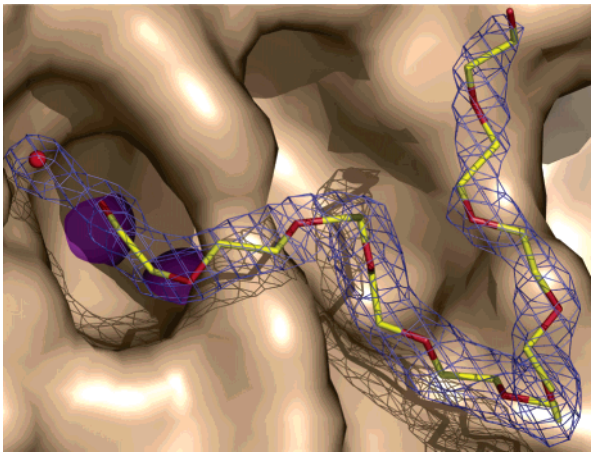

FIGURE 4: Poly(ethylene glycol) (PEG) bound at the active site cleft of [MgMg(APPro)]. Electron density ($2F_O - F_C$, blue, 1σ) and the final refined model of PEG are shown. The solvent-accessible surface of APPro is shown in pale brown, and the active site Mg(II) atoms are shown as magenta spheres.

and the side chains of A439 and D440 were not modeled since there was insufficient electron density to permit an unambiguous interpretation. Two 2-propanol molecules are bound to each subunit in the same positions as observed in [*apo*(APPro)].

There is only a single Ca(II) atom bound at the active site (Figure 3F). It lies in approximately the same position as Mn_A (the M_A site). In all six independent molecules, the Ca(II) atom is bound to $O^{\delta 2}$(Asp271), $N^{\epsilon 2}$(His354), $O^{\epsilon 1}$(Glu383), and $O^{\epsilon 2}$(Glu383), $O^{\epsilon 2}$(Glu406), and a water molecule (W_B) located ~1 Å from the position of M_B in [MnMn(APPro)] and [MgMg(APPro)]. W_B forms hydrogen bonds with the carboxylate side chains of Asp260, Asp271, and Glu406. The interaction with Asp260 is probably a three-centered hydrogen bond. As observed for W_A in [*apo*(APPro)], three protons are required to fulfill the hydrogen-bonding requirements of W_B, and it is likely that one of the carboxylate side chains is protonated. In two APPro molecules (C and E), a second water molecule occupies a position close to that of the axial solvent W2 in [MnMn(APPro)], with the result that the Ca(II) atom in these molecules is seven-coordinate with a distorted pentagonal bipyramidal geometry. The metal−ligand distances and coordination number are consistent with the values expected for Ca. The CBVSs calculated for monomers C and E, 2.3 and 2.1, are equal to the expected value of 2.0 within the limits of precision (*42*). In the other APPro molecules (A, B, D, and F), the seventh (solvent) ligand of the Ca atom could not be modeled due to the absence of significant interpretable electron density. VECSUM (*42*) values, which approach 0 for ideal coordination geometry, are higher in monomers A, B, D, and F (0.41, 0.35, 0.37, and 0.33) than in monomers C and E (0.17 and 0.23), consistent with incomplete coordination spheres for the Ca(II) atoms of monomers A, B, D, and F.

The Structure of Na__ APPro. Unlike previously determined structures of APPro in the tetragonal space group, crystals of [Na__(APPro)] were grown in the presence of the buffer sodium citrate rather than sodium cacodylate. The final model contains one atom of sodium, Na_A, located in the M_A site and one solvent molecule, W_B, in a position close to the M_B site (Figure 3G). The presence of one Na(I) atom and one solvent molecule, rather than two Mg(II) atoms, at the active site was inferred from the metal−ligand and solvent−ligand distances (2.3−2.6 Å for the Na and 2.4−2.7 Å for the solvent rather than 2.0−2.2 Å as is typical for Mg (*43*)), the lack of evidence of axial solvent molecules (W2 and W3), and an Na_A−W_B distance (2.7 Å) too short for the presence of a second metal atom. Na_A has a distorted octahedral geometry. The CBVS for the Na atom is 1.5 compared with the expected value of 1.6 (*42*), confirming that the metal is sodium. The interactions between W_B and the protein are identical to those observed for W_B in [Ca__(APPro)]. While the solvent structure in the active site is significantly rearranged, the positions of protein ligands do not differ significantly from the positions of equivalent residues in [MnMn(APPro)].

The Structure of Apo APPro in Complex with Substrate. Crystals of [*apo*(APPro)] bound to substrate were made by soaking [Na__(APPro)] crystals in fresh mother liquor supplemented with ValProLeu for 1 h. After initial positional refinement, strong difference electron density at the active site could be modeled as the tripeptide ValProLeu. Unexpectedly, there was no evidence for metal atoms at the active site (Figure 5A).

The ValProLeu tripeptide is located at the active site of the enzyme and forms sufficient hydrogen bonds with the protein to satisfy all potential hydrogen-bond donors or acceptors (Figures 5A and 6A). The N(amino) atom of the substrate Val residue is equidistant from the positions occupied by Mn_B and W1 in the structure of [MnMn(APPro)], forming bifurcated hydrogen bonds with the carboxylate side chains of Asp260 and Aps271. The O(peptide) atom of the substrate Val residue forms a hydrogen bond with $N^{\epsilon 2}$(His361). The side chain of the substrate Val residue makes van der Waals contacts with the side chains of residues Tyr229 and His243. The substrate Pro residue lies in a pocket lined by the side chains of residues His350, Arg404, and Leu242. The O(peptide) atom of the substrate Pro residue forms a hydrogen bond with $N^{\epsilon 2}$(His243). The imidazole side chain of His243, often not well-resolved in electron density in APPro structures, is clearly visible in this structure. The substrate Leu residue is located in the wide opening of the substrate binding cleft of APPro, the N(peptide) atom forming a hydrogen bond with a solvent molecule that in turn hydrogen bonds to $O^{\epsilon 2}$(Glu383), and the O(peptide) atom of Gly351. One O(carboxylate) atom of the substrate Leu residue forms a hydrogen bond with $N^{\eta 2}$(Arg153) from an adjacent subunit (generated by the symmetry operation [$y - 1$, $1/2 + x$, $1/2 - z$]), and the other forms hydrogen bonds with $N^{\eta 2}$(Arg370) and with the N(peptide) atom of Gly351. The side chain of the substrate Leu residue makes van der Waals contacts with C^{β}(His354). The residues in and around the active site of APPro do not require significant rearrangement to accommodate bound substrate.

The Structure of MgMg APPro in Complex with Product. Crystals of [MgMg(APPro)] complexed with the product dipeptide ProLeu were made by soaking [Na__(APPro)] crystals in fresh mother liquor containing the substrate ValProLeu for 20 h. Positive difference electron density at the active site was interpreted as bound product, ProLeu, and metal atoms at both the M_A and M_B sites (Figure 5B). The N(amino) atom of the product Pro makes a hydrogen

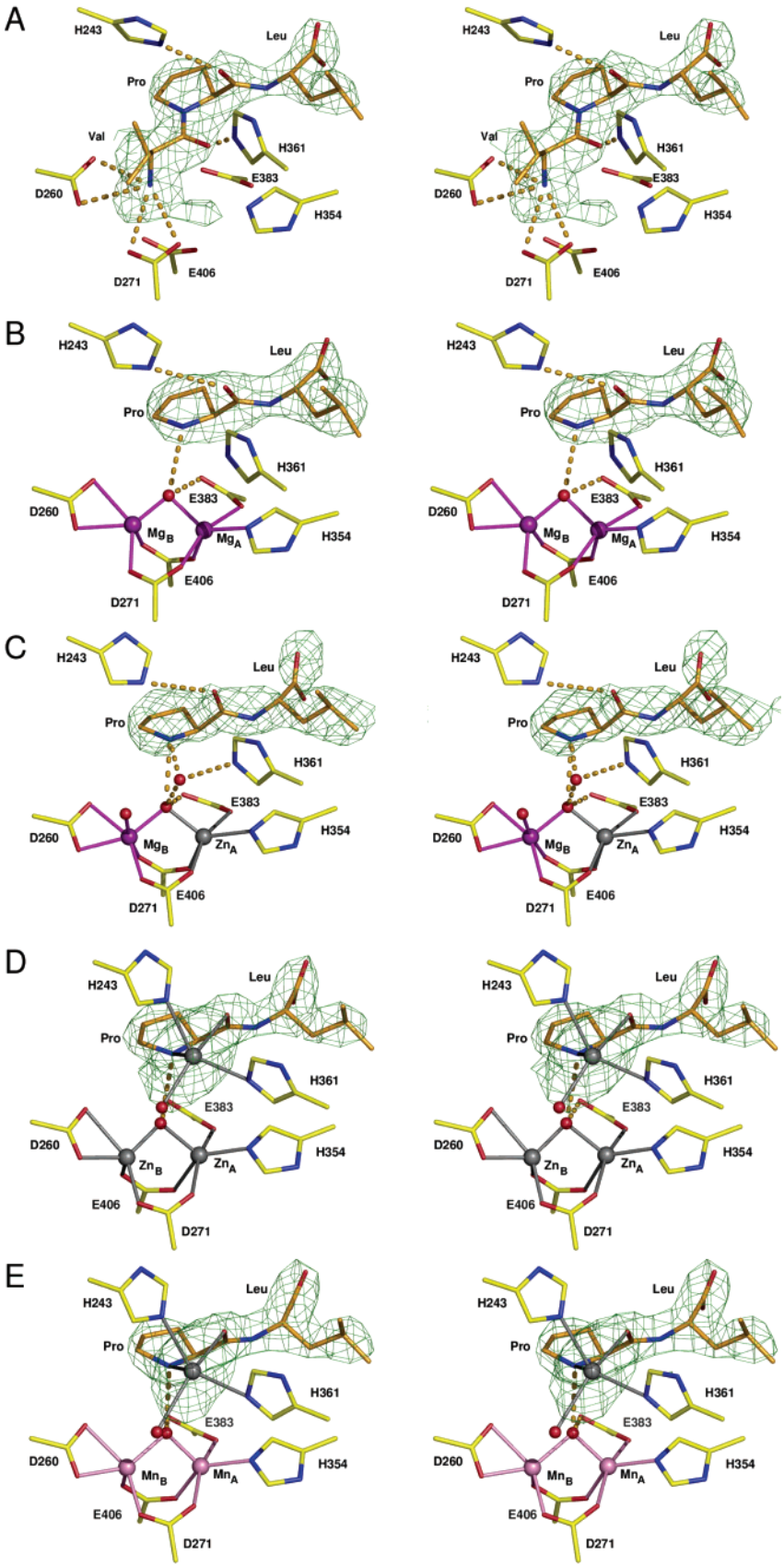

FIGURE 5: Stereoviews showing the active site of *E. coli* APPro with substrate (ValProLeu) or product (ProLeu) bound in the presence of different metals. $F_O - F_C$ difference electron density calculated before the substrate or product was added to the model is shown in green (4σ for A, D, and E; 3σ for B and C). (A) [*apo* (APPro) + ValProLeu]; (B) [MgMg(APPro) + ProLeu]; (C) [ZnMg(APPro) + ProLeu]; (D) [ZnZn(APPro) + Zn, ProLeu]; and (E) [MnMn (APPro) + Zn, ProLeu].

bond with the bridging hydroxide ion, confirming that the N-terminal Val of the original peptide has been removed. The metal atoms were identified as Mg(II) from the metal−ligand distances.

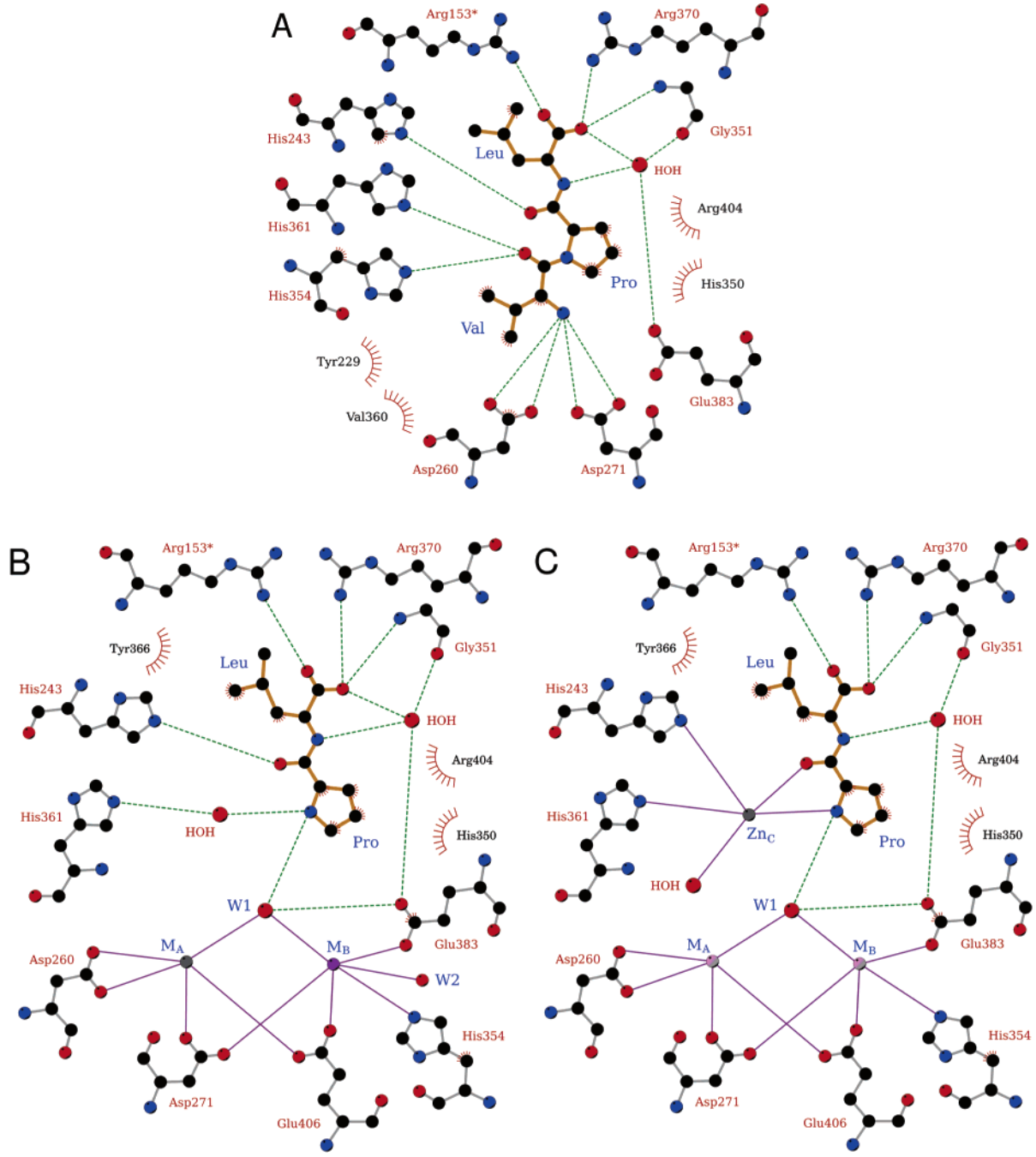

FIGURE 6: Two-dimensional schematic diagrams showing interactions between APPro and either substrate or product. Hydrogen bonds (green dashes), metal−ligand bonds (magenta lines), and hydrophobic interactions (red combs) are shown. The * denotes residue in neighboring subunit. (A) ValProLeu in [*apo*(APPro) + ValProLeu]; (B) ProLeu in [MgMg(APPro) + ProLeu] or [ZnMg(APPro) + ProLeu]; and (C) ProLeu in [MnMn(APPro) + Zn, ProLeu] or [ZnZn(APPro) + Zn, ProLeu]. Figures were prepared using LIGPLOT (*62*).

The dipeptide ProLeu is in the same position as in the published structure of [MnMn(APPro) + ProLeu] (*4*). The bridging solvent molecule (W1) forms a hydrogen bond with the N(amino) atom of the product Pro residue. A second solvent molecule, which forms hydrogen bonds with the N(amino) atom of the product Pro residue and $N^{\epsilon 2}$(His361), as seen in [MnMn(APPro) + ProLeu] (*4*) and [ZnMg(APPro) + ProLeu] (see below), is not sufficiently well-resolved to allow reliable modeling. The imidazole ring of His243 is well-ordered, the $N^{\epsilon 2}$ atom making a weak hydrogen bond interaction (3.2 Å) with the O(peptide) atom of the product Pro residue. The solvent molecule that makes a hydrogen bond with the N(peptide) atom of the substrate Leu in the published [Mn,Mn(APPro) + ProLeu] structure is not visible in this structure.

The Structure of ZnZn APPro. Crystals of [ZnZn(APPro)] were made by soaking [Na_(APPro)] crystals in fresh mother liquor with 1 mM $ZnCl_2$ for 2 h. Two strong positive peaks in difference electron density were evident at the active site after initial positional refinement and were modeled as two atoms of Zn(II) (Figure 3D). The presence of two anomalous peaks at the active site with integrated heights of 94 and 101 (compared with 75 for the strongest sulfur anomalous peak, S^{δ}(Met19)) confirms the identity of the atoms as Zn (*f*″: Zn 0.7 e^-, S 0.6 e^-, Mg 0.2 e^-, and Na 0.1 e^- at $\lambda = 1.54$ Å (*44*)).

The two atoms of Zn(II) at the active site occupy positions equivalent to those of the two Mn(II) atoms in [MnMn-(APPro)]. The Zn−ligand and Mn−ligand distances are very similar (Figure 3A,D). The Zn_A-Zn_B distance, 3.1 Å, is not significantly shorter than the Mn_A-Mn_B distance, 3.3 Å. The hydrogen bond between the bridging solvent molecule (W1) and $O^{\epsilon 1}$(Glu383) is longer in this structure, 2.9 Å, than the equivalent bond in the native structure, 2.5 Å. The two axial solvent molecules (W2 and W3) seen in the native structure are not present in this structure, and both Zn_A and Zn_B are five-coordinate. Zn_A has a trigonal bipyramidal coordination, while Zn_B is best described as having a square pyramidal coordination.

In addition to the active site Zn atoms, two Zn atoms remote from the active site have been identified. Electron density at these additional sites is observed only when Zn^{2+} has been added to the crystals. One of the additional Zn atoms (Zn_D) is located near the junction of the N- and C-terminal domains. Only two ligands of Zn_D are resolved in the electron density, namely, $N^{\epsilon 2}$(His170) at 2.0 Å and $O^{\delta 2}$(Asp48) at 2.1 Å. The side chains of these two residues have the same conformations as in [MnMn(APPro)] where they interact directly with each other via a 2.8 Å hydrogen bond between the $N^{\epsilon 2}$ and $O^{\delta 2}$ atoms. The second additional Zn atom (Zn_E) is located at one end of the N-terminal domain, remote from the C-terminal domain and from any symmetry-related molecules. Zn_E has occupancy 0.5 and is highly disordered ($B = 110$ Å^2) with only one ligand visible in electron density, $N^{\epsilon 2}$(His71) at 2.0 Å.

Difference electron density at the active site was modeled as a disordered molecule of MPD. The tertiary alcohol moiety of the bound MPD molecule is in the same location as the prolidyl ring of the ProLeu dipeptide in ProLeu structures, one end of the PEG molecule in [*apo*(APPro)], and the active site 2-propanol molecule in [MgMg(APPro)]. In this structure and in structures with bound ProLeu, a solvent molecule at the active site forms hydrogen bonds with $N^{\epsilon 2}$(His361), with the bridging solvent molecule (W1), and with either the tertiary alcohol of MPD or the N(amino) atom of Pro.

The Structure of ZnZn APPro in Complex with Product. To investigate the binding mode of substrate to [ZnZn-(APPro)], crystals of [ZnZn(APPro)] were soaked with 10 mM ValProLeu for 30 min at 4 °C. Initial refinement of this structure showed that the ValProLeu substrate had been almost fully hydrolyzed to ProLeu in the crystal and that an extra atom of Zn was bound at the active site. The active site appeared to contain a mixture of ValProLeu or ProLeu and the additional Zn atom. The moderate resolution of the data did not allow the refinement of this mixture (Table 1).

To characterize the species containing ProLeu and the additional Zn atom, crystals of [ZnZn(APPro)] in complex with ProLeu were prepared by soaking [Na_(APPro)] crystals in fresh mother liquor with 1 mM $ZnCl_2$ and 10 mM ProLeu for 2 h at 4 °C. The refined structure contains one molecule of ProLeu and three atoms of Zn(II) at the active site. Two of the atoms occupy the normal M_A and M_B sites (Zn_A and Zn_B). A third Zn atom (Zn_C) is in a previously unobserved site (Figure 5D). The displacement parameter of Zn_C refines to a high value ($B = 75$ Å^2 versus 46 Å^2 and 47 Å^2 for Zn_A and Zn_B, respectively), indicating that this atom is disordered or that the site is partially occupied. The metal atoms were modeled as Zn(II) based on the relative height of electron-density peaks and the presence of significant anomalous difference electron-density peaks (Zn_A 105, Zn_B 100, and Zn_C 51 compared with 89 for the strongest sulfur anomalous peak, S^{γ}(Cys263)). The peak for Zn_C is smaller due to the high *B* value for this atom. We note that the only metal ions present in the crystal buffer were Zn^{2+}, Mg^{2+}, and Na^{+}.

The positions of Zn_A and Zn_B, and all their ligands, are indistinguishable from the positions of equivalent atoms in [ZnZn(APPro)]. The molecule of ProLeu occupies the same position as in the complex with Mn ([MnMn(APPro) + ProLeu], PDB ID 1A16 (*4*)). Zn_C is in a pocket formed by the enzyme and the bound dipeptide product ProLeu. The Zn_C ligands are $N^{\epsilon 2}$(His243), $N^{\epsilon 2}$(His361), the N(amino) and O(peptide) atoms of the product Pro residue, and a solvent molecule (Figures 5D and 6C). The imidazole side chain of His243 is rotated 54° around the $C^{\beta}-C^{\gamma}$ bond compared with the equivalent side chain in the published structure of [MnMn(APPro) + ProLeu] (*4*), while the imidazole ring of His361 occupies a position similar to that of the equivalent residue in [MnMn(APPro) + ProLeu].

As in [ZnZn(APPro)], a fourth remote Zn atom (Zn_E) is bound to $N^{\epsilon 2}$(His71). Zn_E is again modeled with half occupancy and is highly disordered ($B = 105$ Å^2). There is no evidence in this structure for Zn_D, the other remote Zn atom present in [ZnZn(APPro)].

The Structure of MnMn APPro in Complex with Product in the Presence of Zn. Crystals of [MnMn(APPro)] in complex with ProLeu and Zn were prepared by soaking [Na_(APPro)] crystals in fresh mother liquor with 1 mM $MnCl_2$, 1 mM $ZnCl_2$, and 10 mM ProLeu for 1 h at 4 °C. The refined structure contains one molecule of ProLeu, two atoms of Mn(II) in the M_A and M_B positions (Mn_A and Mn_B), and one Zn(II) atom (Zn_C). The atoms Mn_A and Mn_B can be identified as Mn, rather than Zn, using their anomalous signals. Mn_A and Mn_B have integrated anomalous peak heights of 167 and 202 (compared with 81 for the strongest sulfur anomalous peak, S^{γ}(Cys263)), much larger than would be expected if Mn_A and Mn_B were replaced by fully occupied Zn atoms (f'': Mn 2.8 e$^-$, Zn 0.7 e$^-$, and S 0.6 e$^-$ at $\lambda = 1.54$ Å (*44*)), although the possibility of some heterogeneity cannot be discounted. The third metal atom, Zn_C, was modeled as Zn and not Mn in view of a small anomalous peak (of height 42) and the fact that the coordination is the same as that of Zn_C in the [ZnZn(APPro) + Zn, ProLeu] structure (see above). Most importantly, in the presence of excess Mn^{2+} (1 mM), the equivalent site in [MnMn(APPro) + ProLeu] is not occupied by a metal atom (*4*). The Zn_C site is only three-quarters occupied and has a large *B* value (70 Å^2), accounting for the small anomalous peak. As in the structure of [ZnZn(APPro) + Zn, ProLeu], Zn_C is disordered. There is no evidence for additional Zn atoms (Zn_D or Zn_E) remote from the active site as in [ZnZn(APPro)].

The coordination of Mn_A and Mn_B in [MnMn(APPro) + Zn, ProLeu] is similar to that in [MnMn(APPro)]. The main difference is that neither of the axial solvent molecules (W2 and W3) is observed, possibly as a result of the lower resolution of the data. The position of the bound product dipeptide ProLeu is identical with that seen in the published structure of [MnMn(APPro) + ProLeu] (*4*). Zn_C and its ligands occupy the same positions as equivalent atoms in [ZnZn(APPro) + Zn, ProLeu] (Figures 5E and 6C).

The Structure of ZnMg APPro. Crystals of [ZnMg(APPro)] were grown from protein overexpressed in *E. coli*, without the addition of metal ions other than Mg^{2+}. The crystals belong to the monoclinic space group *C*2. A structure of APPro has not previously been described in this space group. There are two dimers in the asymmetric unit. The four protein chains are designated A, B, C, or D in the deposited coordinates. Tetramers (more properly dimers-of-dimers) of APPro are formed by the operation of a crystallographic two-fold axis on each dimer. Chain C makes no crystal contacts other than those within the tetramer. Parts or all of the C-terminal residues A440, B439−440, C439−440, and D439−440 were not located in significant electron density and were omitted from the final model. The four independent molecules are not significantly different from one another, reflecting the use of noncrystallographic symmetry restraints in the refinement. Pairwise rms differences over 438 C^{α} atoms range from 0.07 to 0.11 Å.

A difference electron-density map clearly indicated the presence of atoms at the M_A and M_B sites, the former being more electron dense than the latter (Figure 3E). An X-ray fluorescence scan of the crystal (not shown) indicated the presence of Zn and the absence of Mn, Co, and Fe. An anomalous difference electron-density map calculated with data recorded above the Zn absorption edge (9673 eV) had one large positive peak at the M_A site. The presence of Zn was confirmed by a second data set, recorded below the Zn absorption edge (9640 eV), which yielded no anomalous difference peak at the M_A site. The second metal ion at the active site was modeled as Mg on the basis of the height of the difference electron-density peak. Partial occupancy by Zn or Mn would have resulted in an anomalous difference peak, which was not observed. Refinement of the two atoms as Zn and Mg gave temperature factors similar to those of the ligating residues. The Zn(II) atom is five-coordinate, with four close ligands (2.1−2.2 Å) and one more distant ligand (2.5 Å). The four close ligands, $O^{\delta 2}$(Asp271), $N^{\epsilon 2}$(His354), $O^{\epsilon 2}$(Glu406), and a water molecule, approximate a trigonal pyramid. The more distant ligand, the $O^{\epsilon 2}$(Glu383), makes the coordination geometry quasi trigonal bipyramidal. The Mg(II) atom is in the same position as Mg_B in [MgMg-(APPro)] and has the same ligands. Two additional ions modeled as Mg^{2+} are located far from the active site in [ZnMg(APPro)]. Each is coordinated by six water molecules in an octahedral arrangement. They lie between protein molecules in the crystal and do not play any role in stabilizing the tetramer.

The Structure of ZnMg APPro in Complex with Product. In the belief that this form of the enzyme would be inactive yet competent to form a substrate complex, crystals of [ZnMg(APPro)] were soaked in the tripeptide substrate ValProLeu. As observed in the structure of [MgMg(APPro) + ProLeu], difference electron density in each of the four independent copies of the molecule in the asymmetric unit clearly indicated the presence of the dipeptide product, ProLeu, bound at the active site (Figure 5C). The ProLeu dipeptide is in the same position at the active site as observed in [MnMn(APPro) + ProLeu] (*4*). A solvent molecule (W2) is 3.2 Å from Zn_A. This solvent was described as the sixth ligand to Mn_A in earlier refinements of APPro (*4*) but was too far from Mn_A to be described as a metal ligand in the published orthorhombic APPro structure (*5*) and in the new refinement of [MnMn(APPro)]. Here, it makes a hydrogen bond to the N(amino) atom of the bound ProLeu dipeptide and is in almost the same position as a water molecule in [MnMn(APPro) + ProLeu] (*4*).

Source of the Zn in [ZnMg(APPro)]. Since crystals of [ZnMg(APPro)] grew from solutions to which no Zn was added at any stage, the origin of the Zn in the enzyme is a matter of interest. The crystals have one molar equivalent of Zn. APPro sample 1, which had not been dialyzed against a metal chelating agent after purification, contained a significant amount of Zn (39.3 μM by ICP-MS) but no detectable Co or Mn. The concentration of protein in the sample was 5.7 mg mL^{-1} (115 μM) as determined by amino acid analysis. Thus, the molar Zn/APPro ratio in the protein sample was 1:3, that is, insufficient to provide the molar equivalent of Zn in the crystalline enzyme. Substoichiometric amounts of Zn have been observed previously to co-purify with recombinant *E. coli* APPro (*9*). We assume that the crystals picked up additional Zn when they were equilibrated overnight in a fresh drop as part of the cryoprotection protocol, since ICP-MS analysis detected a low level of Zn (1.8 μM) in the reservoir solution. Although the component of reservoir solution responsible for Zn contamination has not been positively identified, it is likely to be the MPD or PEG. No Zn contamination of Tris buffers was detected by ICP-MS.

DISCUSSION

Metal Binding at the Active Site of APPro. The overall structure of APPro is essentially unchanged upon metal binding at the active site and is not sensitive to either the number of metal atoms (zero, one, or two) or their nature. There are local differences in the region surrounding the metal atoms, particularly with respect to the bound solvent molecules.

In the structures where APPro has two metal atoms bound at the active site ([MnMn(APPro)], [MgMg(APPro)], [ZnZn-(APPro)], and [ZnMg(APPro)]), the metal atoms are coordinated by the side chains of residues Asp260, Asp271, His354, His383, and Glu406. There are only small variations in the bond lengths to these ligands (Figure 3A,C−E). In all four structures, a bridging solvent molecule (W1) occupies the same location between the two metal atoms. The positions of the other solvent molecules around the metals are not conserved. In [MgMg(APPro)], W2 and W3 are located sufficiently close to each metal atom to be considered as ligands, resulting in distorted octahedral geometries for both Mg_A and Mg_B. In [MnMn(APPro)] and [ZnMg(APPro)], the solvent molecule W2 is too far (>2.8 Å) from the metal atoms to be a ligand, so that Mn_A and Zn_A have distorted square pyramidal and trigonal bipyramidal geometries, respectively. The position of W3 is unchanged, giving Mn_B and Mg_B distorted octahedral geometries. In [ZnZn(APPro)], neither W2 nor W3 is present and both metal atoms are five-coordinate with distorted trigonal bipyramidal (Zn_A) and square pyramidal (Zn_B) geometries.

When APPro has only one metal atom (M_A) at the active site ([Na_(APPro)] and [Ca_(APPro)]), the ligating groups are the side chains of residues Asp271, His354, His383, and Glu406. Na_A has a distorted octahedral geometry, while the geometry of Ca_A is best described as pentagonal bipyramidal.

In both structures, a water molecule (W_B) occupies the otherwise vacant M_B metal-binding site. In [Na_(APPro)], a solvent molecule (W1) coordinates the metal atom (Na_A) and makes a hydrogen bond to W_B. The $Na_A\cdots W1$ and the $W1\cdots W_B$ distances, 2.6 and 2.7 Å, are longer than in the dinuclear APPro structures cited above. From the geometry, it is reasonable to assume that W1 in [Na_(APPro)] is a water molecule and not a hydroxide ion. In [Ca_(APPro)], no solvent molecule occupies the position of the bridging solvent in the dinuclear structures. Furthermore, the carboxylate side chain of Glu383 acts as a bidentate ligand to Ca_A, in contrast with the dinuclear metal sites, where it acts as a monodentate ligand to M_A and makes a hydrogen bond with the bridging solvent molecule. An additional solvent molecule (W2) coordinates Ca_A making the Ca(II) seven-coordinate. The limited resolution of the [Ca_(APPro)] structure prevented this solvent molecule from being modeled reliably in all six subunits.

When no metals are bound to APPro ([*apo*(APPro)]), two solvent molecules are located at the active site. One solvent molecule (W_A) is in the M_A site. The other solvent molecule (W_B) is disordered and lies between the side chains of Asp260 and Glu383.

APPro Has One 'Tight' and One 'Loose' Metal-Binding Site. The ligand residues that define the two metal-binding sites at the active site of APPro do not reflect the pseudo two-fold symmetry of the 'pita-bread fold'. M_A is coordinated by carboxylate groups from Asp and Glu residues and by an imidazole group from a His residue. M_B, on the other hand, is coordinated exclusively by carboxylate groups of Asp and Glu residues. In MetAP, which has the same set of metal ligands as APPro, isothermal titration calorimetry studies have shown that one active site metal atom is bound much more tightly than the other (K_d (Co_A) = 6.5 μM; K_d (Co_B) > 100 μM) (*45*). The 'tight' metal-binding site, M_A, is the one that includes the imidazole ligand (*21*, *45*).

Although similar metal-binding studies have not been conducted for APPro, the structures described in this paper are consistent with the presence of 'tight' and 'loose' binding sites. In both [Ca_(APPro)] and [Na_(APPro)], the single metal atom is in the 'tight' (M_A) metal-binding site. In the structure with mixed metals, [ZnMg(APPro)], the Zn(II) atom occupies the 'tight' (M_A) metal-binding site and the Mg(II) atom occupies the 'loose' (M_B) metal-binding site. The fact that metal sites M_A and M_B are consistently occupied by Zn(II) and Mg(II), respectively, and not by an average of the two atom types highlights the selectivity of metal binding. We recall that, during the crystallization of [ZnMg(APPro)], Zn^{2+} was present in substoichiometric (low micromolar) amounts, while Mg^{2+} was present in large excess (200 mM).

APPro Retains Activity in Crystals. Attempts to prepare substrate complexes of APPro by soaking crystals of [MnMn(APPro)] in solutions containing ValProLeu always yielded ProLeu bound at the active site regardless of which crystal form of the protein was used (unpublished observations). We therefore attempted to use some of the inactive metal derivatives of APPro characterized in this paper to prepare an enzyme−substrate complex. APPro sample 1 showed no significant enzymatic activity either under standard assay conditions or in the presence of additional Zn or Mg (data not shown). It was therefore surprising to find that crystals of [ZnMg(APPro)] that had been soaked overnight with ValProLeu contained only the product of the hydrolysis reaction, ProLeu. The activity of [ZnMg(APPro)] in the crystals could be reproduced in solution by using high concentrations of enzyme to simulate the conditions in the crystals (data deposited as Supporting Information). As APPro is not activated by Zn (see below), it is likely that Mn or Co contamination, at levels below the detection limit of sensitive techniques such as ICP-MS, is responsible for the observed activity. Given the extreme conditions under which it is observed, this residual level of activity is not physiologically relevant.

Similarly, EGTA-dialyzed APPro (sample 3) crystallized in the presence of 200 mM Mg^{2+} and 300 mM Na^+ displayed some residual activity. After the crystals were soaked for 24 h in the presence of 10 mM ValProLeu, the product dipeptide ProLeu and two Mg(II) atoms were found at the active site. Given that Mg^{2+} is not able to activate APPro (Figure 1A) and that Mg apparently cannot occupy the active site at the same time as substrate (see below), the cleavage of ValProLeu to ProLeu and Val may again be ascribed to a very low level of intrinsic activity or an undetectable level of contamination. Two Mg(II) atoms are present at the active site after the addition of the tripeptide substrate ValProLeu to crystals that originally contained only one atom of Na(I) at the active site. The Mg, which is present in all the crystal-soaking buffers, may be stabilized by the presence of the ProLeu at the active site.

Metal Requirements for the Activity of APPro. Like all enzymes, APPro must bind its substrate in a productive orientation prior to the catalytic step. For peptide hydrolysis to occur, a nucleophile must be positioned for attack on the C(peptide) atom of the scissile bond. Structures of MetAP complexed with inhibitors (*46*) and of APPro with the product inhibitor ProLeu (*4*) have defined the location of substrate binding and have implicated a solvent molecule, which bridges the two metal atoms, as the nucleophile. The postulated role of the metal atoms is the polarization of the bridging solvent molecule with the resulting formation of a hydroxide ion (*23*). The hydroxide acts as the nucleophile in the hydrolysis of Xaa-Pro-peptide by attacking the substrate carbonyl carbon atom. This leads to the formation of a tetrahedral *gem*−diol intermediate that is cleaved to give the products, an amino acid Xaa and the Pro-peptide (*23*).

In the absence of metals, [*apo*(APPro)] can bind the substrate, ValProLeu, in the same location as the inhibitor, ProLeu (Figure 6). APPro was originally identified as a metal-dependent enzyme, and removal of divalent metal ions by EDTA eliminated activity (*8*). The *apo* enzyme lacks the means to generate a nucleophile by polarizing a solvent molecule. The activity of [*apo*(APPro)] can be restored by the addition of divalent metal atoms such as Mn^{2+} (*8*).

Mg(II) and Mn(II) atoms are bound at the active site of APPro in a very similar manner, yet Mn(II) activates APPro while Mg(II) does not. A likely reason is that APPro has a higher affinity for Mn(II) than for Mg(II). In the presence of 1 mM Mn^{2+} and 200 mM Mg^{2+}, only Mn(II) is bound at the active site. Further, when crystals of [Na_(APPro)] are soaked for 1 h in the presence of 300 mM Na^+, 200 mM Mg^{2+}, and 10 mM ValProLeu, the result is [*apo*(APPro) + ValProLeu]; the tripeptide has competed successfully against both Na and Mg for the active site. The two metal ions are obviously bound by APPro with significantly lower affinity

than ValProLeu ($K_M \sim 1$ mM (*47*)). We conclude that the enzyme binds neither Na nor Mg in the presence of substrate and that a physiological role for Mg binding to APPro is therefore very unlikely. Proteins and enzymes generally bind Mg weakly (*48*). The Mg−Mg distance in [MgMg(APPro)] is 3.3 Å. In other enzymes where dinuclear Mg(II) centers are bridged by one or more carboxylate groups, the Mg−Mg distances range from 3.0 to 5.0 Å, the majority being greater than 3.5 Å (*49*−*51*). It is possible that the arrangement of ligands at the active site of APPro, ideal for Mn(II) but less than optimal for Mg(II), contributes to the weak binding of Mg.

In [Ca_(APPro)], Ca(II) is bound at the 'tight' metal-binding site and is coordinated by several solvent molecules, yet it fails to activate the enzyme. The polarizing effect of Ca^{2+} is much weaker than that of Mn^{2+} (Table 2.2 in ref *52*). However, Ca(II) has been reported to polarize a solvent molecule sufficiently to act as a nucleophile in other enzymes such as the secreted form of phospholipase A_2 (*53*), and it has been reported that Ca(II) activates porcine cytosolic APPro (*54*). We assume that in *E. coli* APPro the potentially nucleophilic water molecule is not polarized sufficiently or that it is not located appropriately for catalysis.

The Zn-loaded enzyme, [ZnZn(APPro)], is inactive in our assay system despite the overall similarity of its structure to that of [MnMn(APPro)], including the presence of the putative nucleophilic bridging hydroxide ion. An earlier report by Yoshimoto et al. (*9*) showed weak activity of recombinant *E. coli* APPro in the presence of 10 μM Zn^{2+} but inhibition at higher Zn^{2+} concentrations. We have shown that Zn^{2+} inhibits the active Mn-loaded form of the enzyme with an IC_{50} of 0.5 μM. To test the hypothesis that Zn-loaded APPro is active but is inhibited by excess Zn^{2+}, we have measured the activity at Zn^{2+} concentrations below the IC_{50} value for the inhibition of the Mn-loaded enzyme. Even at these very low Zn^{2+} concentrations, we did not observe any activity. We have no structural explanation for the inactivity of [ZnZn(APPro)] in the absence of excess Zn^{2+}.

The Inhibition of APPro by Zn. As stated above, Zn^{2+} strongly inhibits fully active Mn-loaded APPro ($IC_{50} = 0.5$ μM, Figure 1C). Assuming that Zn^{2+} inhibits Mn-loaded APPro by displacing the active site Mn(II) atoms, the relative concentrations of the two metals in the assay would imply that APPro binds Zn(II) much more tightly than Mn(II). This is not the case; crystals of [MnMn(APPro) + Zn, ProLeu], which have been soaked in equal concentrations of Mn^{2+} and Zn^{2+} (1 mM $MnCl_2$ and 1 mM $ZnCl_2$) have only Mn(II) in the M_A and M_B sites. We conclude that, even under conditions of relatively high concentrations of Zn^{2+}, Zn does not displace Mn from the active site.

The structures of [(ZnZn(APPro) + Zn, ProLeu] and [MnMn(APPro) + Zn, ProLeu] provide an alternate explanation for the inhibition of APPro by Zn. In each of the structures, an additional Zn(II) atom (Zn_C) near the active site is bound directly to the protein and to the ProLeu dipeptide. Zn_C is coordinated by the N(amino) and O(peptide) atoms of the P_1' Pro, the $N^{\epsilon 2}$ atoms of His243 and His361, and a solvent molecule. Zn_C could not be bound if substrate were present in the active site, since the Zn coordinates to the N(amino) atom of the dipeptide product and actually occupies the space required for the P_1 residue. No metal atoms are seen at this location in ProLeu complexes crystallized in the absence of excess Zn^{2+} ([MnMn(APPro) + ProLeu] (*4*), [MgMg(APPro) + ProLeu], and [ZnMg(APPro) + ProLeu]) nor are they seen in the presence of excess Zn^{2+} and in the absence of ProLeu ([ZnZn(APPro)]). Since the enzyme binds Zn_C only in the presence of product, it may stabilize the product-bound form of the enzyme and enhance product inhibition.

His243, a Catalytically Important Residue, Responds to the Contents of the Active Site. His243 is the active site residue with the largest differences in observed conformation among the structures presented in this paper. The conformations differ by rotation of the imidazole group around the $C^{\beta}-C^{\gamma}$ bond. The different conformations do not correlate with different metal atoms at the active site, but rather respond to the contents of the S_1 and S_1' substrate binding sites. His243 is not well-ordered in the absence of exogenous ligands. However, it is ordered and forms hydrogen bonds to bound ProLeu or bound 2-propanol or acts as a ligand to Zn_C bound at the active site.

His243 has previously been identified as important for the catalytic activity of APPro, although the precise nature of its role in catalysis is unclear (*4*, *6*). Mutation of His243 to Ala eliminates APPro activity (unpublished results), and mutation of the equivalent His residue to Ala in MetAP renders MetAP inactive (*55*). It has been proposed that His243 forms a hydrogen bond to the P_1' N(peptide) atom during catalysis in the mechanism of 'pita-bread' metalloenzymes (*23*). This is obviously not possible for APPro as the P_1' residue is always proline, which lacks a proton to form the proposed hydrogen bond. The same is true for prolidase and for the reaction of MetAP with substrates that have proline as a second residue (*56*). The precise role of His243 in APPro therefore remains an interesting question for further study.

The APPro Active Site Cleft Possesses a Hydrophobic Pocket That Binds Proline. The position of the specificity-conferring P_1' Pro residue is identical in the structures of the substrate-bound ([*apo*(APPro) + ValProLeu]) and the product-bound ([MgMg(APPro) + ProLeu], [ZnMg(APPro) + ProLeu], [MnMn(APPro) + Zn, ProLeu], and [ZnZn(APPro) + Zn, ProLeu]) APPro. This Pro residue occupies a shallow hydrophobic pocket lined by residues Leu242, His243, Asp260, His350, Glu383, and Arg404 (the S_1' site, Figure 6). These residues, with the exception of Leu242 and His350, are conserved in all currently available APPro and prolidase sequences. Leu242 is conservatively substituted by other hydrophobic residues (Ile, Met, and Pro), and His350 is replaced by Ala in APPro from *Streptomyces lividans* and *Streptomyces coelicolor*. With the exception of His243, which rotates about the $C^{\beta}-C^{\gamma}$ bond (see above), the positions of the S_1' residues are the same in the all structures presented in this paper, regardless of the contents of the active site.

In several of the structures that have no substrate or product bound at the active site, buffer components are found in the hydrophobic S_1' pocket. In [*apo*(APPro)], two ethylene carbons and an ether oxygen (C1, C2, and O2) of a bound PEG molecule occupy exactly the same positions as the C^{β}, C^{γ}, and C^{δ} atoms, respectively, of bound Pro. In [MgMg(APPro)], a 2-propanol molecule is located in the S_1' pocket with one methyl group occupying the position of the C^{γ} of bound Pro. Finally, in [ZnZn(APPro)], a bound molecule of

MPD occupies the S_1' pocket with one methyl group located between the C^β and C^δ atoms of bound Pro.

APPro and prolidase are so named because they are proline-specific enzymes. The specificity may result from the binding affinity of the enzyme for its substrate or from an inability to cleave non-Pro containing peptides. The P_1' Pro residue in substrate- and product-bound APPro structures occupies a hydrophobic pocket, thereby defining the S_1' binding site of the active enzyme. Structures of APPro where hydrophobic buffer components occupy this pocket show that the S_1' binding site is not uniquely selective for prolidyl rings but is able to accommodate methyl and ethylene glycol groups. Taken together, the present structures partly explain the absolute requirement of APPro for Pro as the second residue of substrate. Hydrophobic P_1' residues larger than Pro or branched at the C^β atom, such as Val, could not be accommodated without a substantial rearrangement of the protein residues that line the S_1' pocket. No such rearrangement is seen in any structures of APPro, indicating that the pocket is quite rigid. Smaller hydrophobic P_1' residues, such as Ala, could be accommodated by the pocket; however, many of the contacts made by Pro in this position would be lost. We propose that the hydrophobic contacts made by the C^γ and C^δ atoms of the P_1' Pro residue to Arg404 are important for stabilizing the interaction between the Pro residue and APPro in the enzyme−substrate complex. The selectivity for proline therefore resides, at least partly, in the binding affinity of APPro for its substrate.

A Model for the Binding of Substrate to 'Pita-Bread' Metalloenzymes in the Presence of a Single Metal Atom. The structure of *apo* APPro in complex with ValProLeu ([*apo*-(APPro) + ValProLeu]) is the first example of substrate bound to a 'pita-bread' metalloenzyme. The structure demonstrates how the enzyme can bind the N-terminus of a substrate even when there is no metal atom in the 'loose' (M_B) metal-binding site. It has been shown that the related enzyme MetAP is active in the presence of only one metal atom at the active site and that the metal is located in the 'tight' (M_A) site (*21*, *22*). In all previously determined structures of 'pita-bread' metalloenzymes with substrate-like inhibitors, transition-state mimics, or N-terminal products, the amino group equivalent to the P_1 amino group of the substrate interacts with a metal atom in the 'loose' (M_B) site (*6*, *46*, *55*, *57*−*59*). The binding mode in these complexes is incompatible with the proposed mechanisms for a single-metal (M_A) active form of *E. coli* MetAP, in which the N(amino) atom of the substrate peptide is not coordinated to a metal atom (Figure 8 of ref *45*; Figure 9 of ref *21*). In the proposed mechanisms, the enzyme−substrate complex is stabilized by a salt bridge from the P_1 N(amino) atom to the carboxylate group of Asp97 in MetAP (equivalent to Asp260 in APPro) and coordination of the P_1 O(peptide) atom to the metal atom in the M_A site (*21*, *45*). Substrate binding may be further stabilized by salt bridges or hydrogen bonds from the N(amino) atom of the substrate peptide to the carboxylate groups of Asp108 and Glu235 (equivalent to Asp271 and Glu406 in APPro, respectively) (*21*). A hydroxide ion coordinated to the metal atom (M_A) is proposed to act as the nucleophile. The structure of *apo* APPro in complex with ValProLeu provides structural support for these models of substrate binding. The ProLeu fragment of the ValProLeu at the active site in [*apo*(APPro) + ValProLeu] is in the same location as the ProLeu in all of the product complexes, confirming this as the likely substrate binding site. The N(amino) atom of the P_1 Val residue forms the proposed hydrogen bonds or salt bridges with Asp260 and Asp271. Further, when [*apo*(APPro) + ValProLeu] and [MnMn(APPro)] are superposed, the 'tight' binding Mn_A atom is located 2.8 Å from the O(peptide) atom of the P_1 Val residue, consistent with the formation of a bond between a metal atom in the M_A site and the P_1 O(peptide) atom.

Concluding Remarks. Taken collectively, this series of APPro structures provides explanations for the inactivity of the Mg-loaded enzyme and the inhibitory role of Zn. As in MetAP, APPro has one 'tight' (M_A) and one 'loose' (M_B) metal-binding site. In the absence of metals at the active site, APPro binds the N(amino) atom of substrate through two of the carboxylate groups that usually bind Mn_B, consistent with models of substrate binding proposed for single-metal active forms of 'pita-bread' metalloenzymes. The functional significance of Mn_B remains an interesting question for future investigations.

ACKNOWLEDGMENT

The authors thank Ms Rita Martinez for crystallization experiments, Dr. Megan Maher, Ms Mihwa Lee, and Dr. Paul Ellis for synchrotron data collection, Drs. Mibel Aguilar and Rebecca Lee for assistance with enzyme kinetics analysis, Dr. Henri Wong for ICP-MS analysis, and Dr. Belinda Sharpe for assistance with peptide synthesis.

SUPPORTING INFORMATION AVAILABLE

Plot of activity of APPro under conditions that mimic those used for crystallization of [ZnMg(APPro) + ProLeu] (Figure S1) and table of metal−ligand bond lengths for all structures (Table S1). This material is available free of charge via the Internet at http://pubs.acs.org.

REFERENCES

1. Simmons, W. H., and Orawski, A. T. (1992) Membrane-bound aminopeptidase P from bovine lung. Its purification, properties, and degradation of bradykinin, *J. Biol. Chem. 267*, 4897−4903.
2. Fraser, C. M., Gocayne, J. D., White, O., Adams, M. D., Clayton, R. A., Fleischmann, R. D., et al. (1995) The minimal gene complement of *Mycoplasma genitalium*, *Science 270*, 397−403.
3. Fleischmann, R. D., Adams, M. D., White, O., Clayton, R. A., Kirkness, E. F., Kerlavage, A. R., et al. (1995) Whole-genome random sequencing and assembly of *Haemophilus influenzae* Rd, *Science 269*, 496−512.
4. Wilce, M. C. J., Bond, C. S., Dixon, N. E., Freeman, H. C., Guss, J. M., Lilley, P. E., et al. (1998) Structure and mechanism of a proline-specific aminopeptidase from *Escherichia coli*, *Proc. Natl. Acad. Sci. U.S.A. 95*, 3472−3477.
5. Graham, S. C., Lee, M., Freeman, H. C., and Guss, J. M. (2003) An orthorhombic form of *Escherichia coli* aminopeptidase P at 2.4 Å resolution, *Acta Crystallogr., Sect. D: Biol. Crystallogr. 59*, 897−902.
6. Graham, S. C., Maher, M. J., Simmons, W. H., Freeman, H. C., and Guss, J. M. (2004) Structure of *Escherichia coli* aminopeptidase P in complex with the inhibitor apstatin, *Acta Crystallogr., Sect. D: Biol. Crystallogr. 60*, 1770−1779.
7. Schechter, I., and Berger, A. (1967) On the size of the active site in proteases. I. Papain, *Biochem. Biophys. Res. Commun. 27*, 157−162.
8. Yaron, A., and Berger, A. (1970) Aminopeptidase-P, *Methods Enzymol. 19*, 521−534.
9. Yoshimoto, T., Tone, H., Honda, T., Osatomi, K., Kobayashi, R., and Tsuru, D. (1989) Sequencing and high expression of ami-

nopeptidase P gene from *Escherichia coli* HB101, *J. Biochem. (Tokyo) 105*, 412−416.
10. Rusu, I., and Yaron, A. (1992) Aminopeptidase P from human leukocytes. *Eur. J. Biochem. 210*, 93−100.
11. Cottrell, G. S., Hooper, N. M., and Turner, A. J. (2000) Cloning, expression, and characterization of human cytosolic aminopeptidase P: a single manganese(II)-dependent enzyme, *Biochemistry 39*, 15121−15128.
12. Orawski, A. T., and Simmons, W. H. (1995) Purification and properties of membrane-bound aminopeptidase P from rat lung, *Biochemistry 34*, 11227−11236.
13. Zhang, L., Crossley, M. J., Dixon, N. E., Ellis, P. J., Fisher, M. L., King, G. F., et al. (1998) Spectroscopic identification of a dinuclear metal centre in manganese(II)-activated aminopeptidase P from *Escherichia coli*: implications for human prolidase, *J. Biol. Inorg. Chem. 3*, 470−483.
14. Hooper, N. M., Hryszko, J., Oppong, S. Y., and Turner, A. J. (1992) Inhibition by converting enzyme inhibitors of pig kidney aminopeptidase P, *Hypertension 19*, 281−285.
15. Ghosh, M., Grunden, A. M., Dunn, D. M., Weiss, R., and Adams, M. W. W. (1998) Characterization of native and recombinant forms of an unusual cobalt-dependent proline dipeptidase (prolidase) from the hyperthermophilic archaeon *Pyrococcus furiosus*, *J. Bacteriol. 180*, 4781−4789.
16. Maher, M. J., Ghosh, M., Grunden, A. M., Menon, A. L., Adams, M. W., Freeman, H. C., et al. (2004) Structure of the prolidase from *Pyrococcus furiosus*, *Biochemistry 43*, 2771−2783.
17. Ben-Bassat, A., Bauer, K., Chang, S. Y., Myambo, K., Boosman, A., and Chang, S. (1987) Processing of the initiation methionine from proteins: properties of the *Escherichia coli* methionine aminopeptidase and its gene structure, *J. Bacteriol. 169*, 751−757.
18. Walker, K. W., and Bradshaw, R. A. (1998) Yeast methionine aminopeptidase I can utilize either Zn^{2+} or Co^{2+} as a cofactor: a case of mistaken identity?, *Protein Sci. 7*, 2684−2687.
19. D'Souza, V, M., and Holz, R. C. (1999) The methionyl aminopeptidase from *Escherichia coli* can function as an iron(II) enzyme, *Biochemistry 38*, 11079−11085.
20. Wang, J., Sheppard, G. S., Lou, P., Kawai, M., Park, C., Egan, D. A., et al. (2003) Physiologically relevant metal cofactor for methionine aminopeptidase-2 is manganese, *Biochemistry 42*, 5035−5042.
21. D'Souza, V, M., Bennett, B., Copik, A. J., and Holz, R. C. (2000) Divalent metal binding properties of the methionyl aminopeptidase from *Escherichia coli*, *Biochemistry 39*, 3817−3826.
22. Cosper, N. J., D'Souza, V, M., Scott, R. A., and Holz, R. C. (2001) Structural evidence that the methionyl aminopeptidase from *Escherichia coli* is a mononuclear metalloprotease, *Biochemistry 40*, 13302−13309.
23. Lowther, W. T., and Matthews, B. W. (2002) Metalloaminopeptidases: common functional themes in disparate structural surroundings, *Chem. Rev. 102*, 4581−4607.
24. Otwinowski, Z. (1993) Oscillation data reduction program, in *Proceedings of the CCP4 Study Weekend: Data Collection and Processing* (Sawyer, L., Isaacs, N., and Bailey, S., Eds.) pp 56−62, SERC Daresbury Laboratory, Warrington, U.K.
25. Jones, T. A., Zou, J. Y., Cowan, S. W., and Kjeldgaard. (1991) Improved methods for building protein models in electron density maps and the location of errors in these models, *Acta Crystallogr., Sect. A: Found. Crystallogr. 47*, 110−119.
26. Emsley, P., and Cowtan, K. (2004) Coot: model-building tools for molecular graphics, *Acta Crystallogr., Sect. D: Biol. Crystallogr. 60*, 2126−2132.
27. Read, R. J. (1986) Improved Fourier coefficients for maps using phases from partial structures with errors, *Acta Crystallogr., Sect. A: Found. Crystallogr. 42*, 140−149.
28. Winn, M. D., Isupov, M. N., and Murshudov, G. N. (2001) Use of TLS parameters to model anisotropic displacements in macromolecular refinement, *Acta Crystallogr., Sect. D: Biol. Crystallogr. 57*, 122−133.
29. Murshudov, G. N., Vagin, A. A., and Dodson, E. J. (1997) Refinement of macromolecular structures by the maximum-likelihood method, *Acta Crystallogr., Sect. D: Biol. Crystallogr. 53*, 240−255.
30. Navaza, J. (1994) AMoRe: an automated package for molecular replacement, *Acta Crystallogr., Sect. A: Found. Crystallogr. 50*, 157−163.
31. Laskowski, R. A., MacArthur, M. W., Moss, D. S., and Thornton, J. M. (1993) *PROCHECK*: a program to check the stereochemical quality of protein structures, *J. Appl. Crystallogr. 26*, 283−291.
32. Vaguine, A. A., Richelle, J., and Wodak, S. J. (1999) SFCHECK: a unified set of procedures for evaluating the quality of macromolecular structure-factor data and their agreement with the atomic model, *Acta Crystallogr., Sect. D: Biol. Crystallogr. 55*, 191−205.
33. Vriend, G. (1990) WHAT IF: a molecular modeling and drug design program, *J. Mol. Graphics 8*, 52−56.
34. Lovell, S. C., Davis, I. W., Arendall, W. B., III, de Bakker, P. I., Word, J. M., Prisant, M. G., et al. (2003) Structure validation by Calpha geometry: phi,psi and Cbeta deviation, *Proteins: Struct., Funct., Genet. 50*, 437−450.
35. Schuttelkopf, A. W., and van Aalten, D. M. (2004) PRODRG: a tool for high-throughput crystallography of protein−ligand complexes, *Acta Crystallogr., Sect. D: Biol. Crystallogr. 60*, 1355−1363.
36. Kleywegt, G. J., and Jones, T. A. (1998) Databases in protein crystallography, *Acta Crystallogr., Sect.* D: *Biol. Crystallogr. 54*, 1119−1131.
37. Kleywegt, G. J., and Jones, T. A. (1997) Detecting folding motifs and similarities in protein structures, *Methods Enzymol. 277*, 525−545.
38. Kleywegt, G. J., Zou, J. Y., Kjeldgaard, M., and Jones, T. A. (2001) Around O, in *International Tables for Crystallography, Volume F. Crystallography of Biological Macromolecules* (Rossmann, M. G., and Arnold, E., Eds.) pp 353−356, 366−367, Kluwer Academic Publishers, Dordrecht, The Netherlands.
39. Stöckel-Maschek, A., Stiebitz, B., Koelsch, R., and Neubert, K. (2003) A continuous fluorimetric assay for aminopeptidase P detailed analysis of product inhibition, *Anal. Biochem. 322*, 60−67.
40. Yoshimoto, T., Murayama, N., Honda, T., Tone, H., and Tsuru, D. (1988) Cloning and expression of aminopeptidase P gene from *Escherichia coli* HB101 and characterization of expressed enzyme, *J. Biochem. (Tokyo) 104*, 93−97.
41. Remington, S. J., Wachter, R. M., Yarbrough, D. K., Branchaud, B., Anderson, D. C., Kallio, K., and Lukyanov, K. A. (2005) zFP538, a yellow-fluorescent protein from *Zoanthus*, contains a novel three-ring chromophore, *Biochemistry 44*, 202−212.
42. Muller, P., Kopke, S., and Sheldrick, G. M. (2003) Is the bond-valence method able to identify metal atoms in protein structures?, *Acta Crystallogr., Sect. D: Biol. Crystallogr. 59*, 32−37.
43. Harding, M. M. (1999) The geometry of metal−ligand interactions relevant to proteins, *Acta Crystallogr., Sect. D: Biol. Crystallogr. 55*, 1432−1443.
44. Arndt, U. W., Brown, P. J., Colliex, C., Cowley, J. M., Creagh, D. C., Dolling, G., et al. (1992) Production and properties of radiations, in *International Tables for Crystallography, Volume C. Mathematical, Physical and Chemical Tables* (Wilson, A. J. C., Ed.) pp219−220, Kluwer Academic Publishers, Dordrecht, The Netherlands.
45. Copik, A. J., Swierczek, S. I., Lowther, W. T., D'Souza, V, M., Matthews, B. W., and Holz, R. C. (2003) Kinetic and spectroscopic characterization of the H178A methionyl aminopeptidase from *Escherichia coli*, *Biochemistry 42*, 6283−6292.
46. Lowther, W. T., Zhang, Y., Sampson, P. B., Honek, J. F., and Matthews, B. W. (1999) Insights in the mechanism of *Escherichia coli* methionine aminopeptidase from the structural analysis of reaction products and phosphorus-based transition-state analogues, *Biochemistry 38*, 14810−14819.
47. Yoshimoto, T., Orawski, A. T., and Simmons, W. H. (1994) Substrate specificity of aminopeptidase P from *Escherichia coli*: comparison with membrane-bound forms from rat and bovine lung, *Arch. Biochem. Biophys. 311*, 28−34.
48. Cowan, J. A. (2002) Structural and catalytic chemistry of megnesium-dependent enzymes, *BioMetals 15*, 225−235.
49. Ye, B.-H., Mak, T., Williams, I. D., and Li, X.-Y. (1998) The first two aqua-bridged dimagnesium (II) complexes: structural models for active sites in dimetallic hydrolases, *J. Chem. Soc., Dalton Trans.* 1935−1936.
50. Black, C. B., Huang, H.-W., and Cowan, J. A. (1994) Biological coordination chemistry of magnesium, sodium and potassium ions. Protein and nucleotide binding sites, *Coord. Chem. Rev. 135/136*, 165−202.
51. Castagnetto, J. M., Hennessy, S. W., Roberts, V. A., Getzoff, E. D., Tainer, J. A., and Pique, M. E. (2002) MDB: the metallo-

protein database and browser at the Scripps Research Institute, *Nucleic Acids Res. 30*, 379−382.
52. Wulfsberg, G. (1991) *Principles of Descriptive Inorganic Chemistry*, University Science Books, Mill Valley,CA.
53. Berg, O. G., Gelb, M. H., Tsai, M. D., and Jain, M. K. (2001) Interfacial enzymology: the secreted phospholipase A_2-paradigm, *Chem. Rev. 101*, 2613−2654.
54. Lloyd, G. S., Hryszko, J., Hooper, N. M., and Turner, A. J. (1996) Inhibition and metal ion activation of pig kidney aminopeptidase P. Dependence on nature of substrate, *Biochem. Pharmacol. 52*, 229−236.
55. Lowther, W. T., Orville, A. M., Madden, D. T., Lim, S., Rich, D. H., and Matthews, B. W. (1999) *Escherichia coli* methionine aminopeptidase: implications of crystallographic analyses of the native, mutant, and inhibited enzymes for the mechanism of catalysis, *Biochemistry 38*, 7678−7688.
56. Walker, K. W., and Bradshaw, R. A. (1999) Yeast methionine aminopeptidase I—alteration of substrate specificity by site-directed mutagenesis, *J. Biol. Chem. 274*, 13403−13409.
57. Copik, A. J., Nocek, B. P., Swierczek, S. I., Ruebush, S., Jang, S. B., Meng, L., et al. (2005) EPR and X-ray crystallographic characterization of the product-bound form of the MnII-loaded methionyl aminopeptidase from *Pyrococcus furiosus*, *Biochemistry 44*, 121−129.
58. Douangamath, A., Dale, G. E., D'Arcy, A., Almstetter, M., Eckl, R., Frutos-Hoener, A., et al. (2004) Crystal structures of *Staphylococcus aureus* methionine aminopeptidase complexed with keto heterocycle and aminoketone inhibitors reveal the formation of a tetrahedral intermediate, *J. Med. Chem. 47*, 1325−1328.
59. Sheppard, G. S., Wang, J., Kawai, M., BaMaung, N. Y., Craig, R. A., Erickson, S. A., et al. (2004) 3-Amino-2-hydroxyamides and related compounds as inhibitors of methionine aminopeptidase-2, *Bioorg. Med. Chem. Lett. 14*, 865−868.
60. Cruickshank, D. W. J. (1999) Remarks about protein structure precision, *Acta Crystallogr., Sect. D: Biol. Crystallogr. 55*, 583−601.
61. DeLano, W. L. (2002) *The PyMOL Molecular Graphics System*, DeLano Scientific, San Carlos, CA.
62. Wallace, A. C., Laskowski, R. A., and Thornton, J. M. (1995) LIGPLOT: a program to generate schematic diagrams of protein−ligand interactions, *Protein Eng. 8*, 127−134.

BI0512849